EUROPEAN ORGANIZATION FOR NUCLEAR RESEARCH

CERN-PPE/95-070
May 5, 1995

Measurement of the $\tau^- \to h^- h^+ h^- \nu_\tau$ and $\tau^- \to h^- h^+ h^- \geq 1\pi^0 \nu_\tau$ branching ratios

The OPAL Collaboration

Abstract

The branching ratios of the $\tau^- \to h^- h^+ h^- \nu_\tau$ and $\tau^- \to h^- h^+ h^- \geq 1\pi^0 \nu_\tau$ decays, where h is either a charged π or K meson, are measured using a data sample of 87861 $\tau^+\tau^-$ pairs collected with the OPAL detector at LEP. The two branching ratios are extracted simultaneously from a sample of three charged particle decays and found to be:

$$\begin{aligned} B(\tau^- \to h^- h^+ h^- \nu_\tau) &= (9.87 \pm 0.10 \pm 0.24)\% \\ B(\tau^- \to h^- h^+ h^- \geq 1\pi^0 \nu_\tau) &= (5.09 \pm 0.10 \pm 0.23)\% \end{aligned}$$

where the first error is statistical and the second systematic. The branching ratio of the τ lepton into three charged particles is measured to be:

$$B(\tau^- \to \text{3-prong}) = (14.96 \pm 0.09 \pm 0.22)\%$$

To be submitted to Zeitschrift für Physik C - Particle and Fields

The OPAL Collaboration

R. Akers[16], G. Alexander[23], J. Allison[16], N. Altekamp[5], K. Ametewee[25], K.J. Anderson[9], S. Anderson[12], S. Arcelli[2], S. Asai[24], D. Axen[29], G. Azuelos[18,a], A.H. Ball[17], E. Barberio[26], R.J. Barlow[16], R. Bartoldus[3], J.R. Batley[5], G. Beaudoin[18], S. Bethke[14], A. Beck[23], G.A. Beck[13], C. Beeston[16], T. Behnke[27], K.W. Bell[20], G. Bella[23], S. Bentvelsen[8], P. Berlich[10], J. Bechtluft[14], O. Biebel[14], I.J. Bloodworth[1], P. Bock[11], H.M. Bosch[11], M. Boutemeur[18], S. Braibant[12], P. Bright-Thomas[25], R.M. Brown[20], A. Buijs[8], H.J. Burckhart[8], R. Bürgin[10], C. Burgard[27], P. Capiluppi[2], R.K. Carnegie[6], A.A. Carter[13], J.R. Carter[5], C.Y. Chang[17], C. Charlesworth[6], D.G. Charlton[1,b], S.L. Chu[4], P.E.L. Clarke[15], J.C. Clayton[1], S.G. Clowes[16], I. Cohen[23], J.E. Conboy[15], O.C. Cooke[16], M. Cuffiani[2], S. Dado[22], C. Dallapiccola[17], G.M. Dallavalle[2], C. Darling[31], S. De Jong[12], L.A. del Pozo[8], H. Deng[17], M.S. Dixit[7], E. do Couto e Silva[12], J.E. Duboscq[8], E. Duchovni[26], G. Duckeck[8], I.P. Duerdoth[16], U.C. Dunwoody[8], J.E.G. Edwards[16], P.G. Estabrooks[6], H.G. Evans[9], F. Fabbri[2], B. Fabbro[21], M. Fanti[2], P. Fath[11], F. Fiedler[12], M. Fierro[2], M. Fincke-Keeler[28], H.M. Fischer[3], R. Folman[26], D.G. Fong[17], M. Foucher[17], H. Fukui[24], A. Fürtjes[8], P. Gagnon[6], A. Gaidot[21], J.W. Gary[4], J. Gascon[18], S.M. Gascon-Shotkin[17], N.I. Geddes[20], C. Geich-Gimbel[3], S.W. Gensler[9], F.X. Gentit[21], T. Geralis[20], G. Giacomelli[2], P. Giacomelli[4], R. Giacomelli[2], V. Gibson[5], W.R. Gibson[13], J.D. Gillies[20], J. Goldberg[22], D.M. Gingrich[30,a], M.J. Goodrick[5], W. Gorn[4], C. Grandi[2], E. Gross[26], G.G. Hanson[12], M. Hansroul[8], M. Hapke[13], C.K. Hargrove[7], P.A. Hart[9], C. Hartmann[3], M. Hauschild[8], C.M. Hawkes[8], R. Hawkings[8], R.J. Hemingway[6], G. Herten[10], R.D. Heuer[8], J.C. Hill[5], S.J. Hillier[8], T. Hilse[10], P.R. Hobson[25], D. Hochman[26], R.J. Homer[1], A.K. Honma[28,a], R. Howard[29], R.E. Hughes-Jones[16], D.E. Hutchcroft[5], P. Igo-Kemenes[11], D.C. Imrie[25], A. Jawahery[17], P.W. Jeffreys[20], H. Jeremie[18], M. Jimack[1], A. Joly[18], M. Jones[6], R.W.L. Jones[8], P. Jovanovic[1], D. Karlen[6], J. Kanzaki[24], K. Kawagoe[24], T. Kawamoto[24], R.K. Keeler[28], R.G. Kellogg[17], B.W. Kennedy[20], B.J. King[8], J. King[13], J. Kirk[29], S. Kluth[5], T. Kobayashi[24], M. Kobel[10], D.S. Koetke[6], T.P. Kokott[3], S. Komamiya[24], R. Kowalewski[8], T. Kress[11], P. Krieger[6], J. von Krogh[11], P. Kyberd[13], G.D. Lafferty[16], H. Lafoux[8], R. Lahmann[17], W.P. Lai[19], D. Lanske[14], J. Lauber[8], J.G. Layter[4], A.M. Lee[31], E. Lefebvre[18], D. Lellouch[26], J. Letts[2], L. Levinson[26], S.L. Lloyd[13], F.K. Loebinger[16], G.D. Long[17], B. Lorazo[18], M.J. Losty[7], J. Ludwig[10], A. Luig[10], A. Malik[21], M. Mannelli[8], S. Marcellini[2], C. Markus[3], A.J. Martin[13], J.P. Martin[18], T. Mashimo[24], W. Matthews[25], P. Mättig[3], J. McKenna[29], E.A. Mckigney[15], T.J. McMahon[1], A.I. McNab[13], F. Meijers[8], S. Menke[3], F.S. Merritt[9], H. Mes[7], A. Michelini[8], G. Mikenberg[26], D.J. Miller[15], R. Mir[26], W. Mohr[10], A. Montanari[2], T. Mori[24], M. Morii[24], U. Müller[3], B. Nellen[3], B. Nijjhar[16], S.W. O'Neale[1], F.G. Oakham[7], F. Odorici[2], H.O. Ogren[12], N.J. Oldershaw[16], C.J. Oram[28,a], M.J. Oreglia[9], S. Orito[24], F. Palmonari[2], J.P. Pansart[21], G.N. Patrick[20], M.J. Pearce[1], P.D. Phillips[16], J.E. Pilcher[9], J. Pinfold[30], D.E. Plane[8], P. Poffenberger[28], B. Poli[2], A. Posthaus[3], T.W. Pritchard[13], H. Przysiezniak[30], M.W. Redmond[8], D.L. Rees[1], D. Rigby[1], M.G. Rison[5], S.A. Robins[13], N. Rodning[30], J.M. Roney[28], E. Ros[8], A.M. Rossi[2], M. Rosvick[28], P. Routenburg[30], Y. Rozen[8], K. Runge[10], O. Runolfsson[8], D.R. Rust[12], M. Sasaki[24], C. Sbarra[2], A.D. Schaile[8], O. Schaile[10], F. Scharf[3], P. Scharff-Hansen[8], P. Schenk[4], B. Schmitt[3], M. Schröder[8], H.C. Schultz-Coulon[10], P. Schütz[3], M. Schulz[8], J. Schwiening[3], W.G. Scott[20], M. Settles[12], T.G. Shears[16], B.C. Shen[4], C.H. Shepherd-Themistocleous[7], P. Sherwood[15], G.P. Siroli[2], A. Skillman[15], A. Skuja[17], A.M. Smith[8], T.J. Smith[28], G.A. Snow[17], R. Sobie[28], S. Söldner-Rembold[10], R.W. Springer[30], M. Sproston[20], A. Stahl[3], M. Starks[12], C. Stegmann[10], K. Stephens[16], J. Steuerer[28], B. Stockhausen[3], D. Strom[19], P. Szymanski[20], R. Tafirout[18], P. Taras[18], S. Tarem[26],

M. Tecchio[9], P. Teixeira-Dias[11], N. Tesch[3], M.A. Thomson[8], E. von Törne[3], S. Towers[6], M. Tscheulin[10], T. Tsukamoto[24], A.S. Turcot[9], M.F. Turner-Watson[8], P. Utzat[11], R. Van Kooten[12], G. Vasseur[21], P. Vikas[18], M. Vincter[28], F. Wäckerle[10], A. Wagner[27], D.L. Wagner[9], C.P. Ward[5], D.R. Ward[5], J.J. Ward[15], P.M. Watkins[1], A.T. Watson[1], N.K. Watson[7], P. Weber[6], P.S. Wells[8], N. Wermes[3], B. Wilkens[10], G.W. Wilson[27], J.A. Wilson[1], T. Wlodek[26], G. Wolf[26], S. Wotton[11], T.R. Wyatt[16], G. Yekutieli[26], V. Zacek[18], W. Zeuner[8], G.T. Zorn[17].

[1]School of Physics and Space Research, University of Birmingham, Birmingham B15 2TT, UK
[2]Dipartimento di Fisica dell' Università di Bologna and INFN, I-40126 Bologna, Italy
[3]Physikalisches Institut, Universität Bonn, D-53115 Bonn, Germany
[4]Department of Physics, University of California, Riverside CA 92521, USA
[5]Cavendish Laboratory, Cambridge CB3 0HE, UK
[6]Carleton University, Department of Physics, Colonel By Drive, Ottawa, Ontario K1S 5B6, Canada
[7]Centre for Research in Particle Physics, Carleton University, Ottawa, Ontario K1S 5B6, Canada
[8]CERN, European Organisation for Particle Physics, CH-1211 Geneva 23, Switzerland
[9]Enrico Fermi Institute and Department of Physics, University of Chicago, Chicago IL 60637, USA
[10]Fakultät für Physik, Albert Ludwigs Universität, D-79104 Freiburg, Germany
[11]Physikalisches Institut, Universität Heidelberg, D-69120 Heidelberg, Germany
[12]Indiana University, Department of Physics, Swain Hall West 117, Bloomington IN 47405, USA
[13]Queen Mary and Westfield College, University of London, London E1 4NS, UK
[14]Technische Hochschule Aachen, III Physikalisches Institut, Sommerfeldstrasse 26-28, D-52056 Aachen, Germany
[15]University College London, London WC1E 6BT, UK
[16]Department of Physics, Schuster Laboratory, The University, Manchester M13 9PL, UK
[17]Department of Physics, University of Maryland, College Park, MD 20742, USA
[18]Laboratoire de Physique Nucléaire, Université de Montréal, Montréal, Quebec H3C 3J7, Canada
[19]University of Oregon, Department of Physics, Eugene OR 97403, USA
[20]Rutherford Appleton Laboratory, Chilton, Didcot, Oxfordshire OX11 0QX, UK
[21]CEA, DAPNIA/SPP, CE-Saclay, F-91191 Gif-sur-Yvette, France
[22]Department of Physics, Technion-Israel Institute of Technology, Haifa 32000, Israel
[23]Department of Physics and Astronomy, Tel Aviv University, Tel Aviv 69978, Israel
[24]International Centre for Elementary Particle Physics and Department of Physics, University of Tokyo, Tokyo 113, and Kobe University, Kobe 657, Japan
[25]Brunel University, Uxbridge, Middlesex UB8 3PH, UK
[26]Particle Physics Department, Weizmann Institute of Science, Rehovot 76100, Israel
[27]Universität Hamburg/DESY, II Institut für Experimental Physik, Notkestrasse 85, D-22607 Hamburg, Germany
[28]University of Victoria, Department of Physics, P O Box 3055, Victoria BC V8W 3P6, Canada
[29]University of British Columbia, Department of Physics, Vancouver BC V6T 1Z1, Canada
[30]University of Alberta, Department of Physics, Edmonton AB T6G 2J1, Canada
[31]Duke University, Dept of Physics, Durham, NC 27708-0305, USA

[a] Also at TRIUMF, Vancouver, Canada V6T 2A3
[b] Royal Society University Research Fellow

1 Introduction

This paper presents a measurement of the branching ratios of the τ lepton into three charged particles (3-prongs) and of the semi-inclusive decays $\tau^- \to h^-h^+h^-\nu_\tau$ and $\tau^- \to h^-h^+h^- \geq 1\pi^0\nu_\tau$, where $h^\pm$ is either a $\pi^\pm$ or $K^\pm$ meson. Such measurements are motivated experimentally by remaining inconsistencies in the experimental data for the τ branching ratios, as discussed by K. Hayes in [1]. In Z^0 decays, τ samples can be selected with high efficiency and low background, thus permitting precise measurements of these 3-prong branching ratios.

Previously published measurements of the $\tau^- \to h^-h^+h^-\nu_\tau$ branching ratio show inconsistencies that are not yet resolved [2, 3]. Although there are no firm theoretical predictions for the branching ratio of τ decays into three charged hadrons, it is known that axial-vector current decays dominate. Perturbative QCD calculations of the axial-vector component of the τ hadronic width predict a branching ratio for the three-pion final states, $\tau^- \to (3\pi)^-\nu_\tau$, of $(18.0 \pm 0.7)\%$ [5].[1] The $\tau^- \to (3\pi)^-\nu_\tau$ channel is known to be dominated by the $a_1(1260)^-$ resonance. Neglecting corrections of order m_π^2/m_τ^2, chiral symmetry predicts that the $a_1(1260)^-$ decays equally into $\pi^-\pi^+\pi^-$ and $\pi^-\pi^0\pi^0$ final states [11]. Ignoring small phase space corrections, this leads to a value for the branching ratio of $\tau^- \to \pi^-\pi^+\pi^-\nu_\tau$ decays of $(9.0 \pm 0.5)\%$, which is higher than the present $\tau^- \to h^-h^+h^-\nu_\tau$ world average of $(8.0 \pm 0.4)\%$ [4]. The discrepancy becomes more significant when one considers the contributions from $\tau^- \to K^-\pi^+\pi^-\nu_\tau$ and $\tau^- \to K^-K^+\pi^-\nu_\tau$ decays [12, 13]. On the other hand, good agreement with the perturbative QCD calculations is found for the symmetric $\tau^- \to \pi^-\pi^0\pi^0\nu_\tau$ decay channel; its branching ratio can be extracted from the measured world average branching ratio $B(\tau^- \to h^-\pi^0\pi^0\nu_\tau) = (9.0 \pm 0.4)\%$ [4], after subtracting the small Cabibbo-suppressed contribution $B(\tau^- \to K^-\pi^0\pi^0\nu_\tau) = (0.05 \pm 0.04)\%$ [6, 7].

The $\tau^- \to h^-h^+h^- \geq 1\pi^0\nu_\tau$ branching ratio benefits from more accurate theoretical predictions and has more consistent experimental results. The dominant contribution to this channel comes from the vector current decay $\tau^- \to \pi^-\pi^+\pi^-\pi^0\nu_\tau$. Assuming the Conserved Vector Current (CVC) hypothesis, one can predict the rate of τ decays to four pions from the $e^+e^- \to 4\pi$ annihilation cross section. Using the e^+e^- results of reference [14], one obtains a value of $(4.8 \pm 0.7)\%$ for the $\tau^- \to \pi^-\pi^+\pi^-\pi^0\nu_\tau$ branching ratio [5], in agreement with other authors' predictions [15]. Other contributions to the semi-inclusive $\tau^- \to h^-h^+h^- \geq 1\pi^0\nu_\tau$ decay come from the observed $\tau^- \to h^-h^+h^-2\pi^0\nu_\tau$ channel [9] and from potential $\tau^- \to h^-h^+h^-3\pi^0\nu_\tau$ decays. A limit on this last contribution can be obtained from CVC predictions for the rate of τ decays to six pions [5]. The sum of these theoretical predictions and experimental results leads to a value for the $\tau^- \to h^-h^+h^- \geq 1\pi^0\nu_\tau$ branching ratio which is in agreement with the present world average value of $B(\tau^- \to h^-h^+h^- \geq 1\pi^0\nu_\tau) = (5.4 \pm 0.4)\%$ [4].

In this analysis, the $\tau^- \to h^-h^+h^-\nu_\tau$ and $\tau^- \to h^-h^+h^- \geq 1\pi^0\nu_\tau$ branching ratios are measured using a data sample of 87861 $\tau^+\tau^-$ pairs collected with the OPAL detector at

[1] In this calculation, the $\tau^- \to (1\pi)^-\nu_\tau$ contribution to the axial-vector hadronic width is estimated on the basis of the inclusive world average $B(\tau^- \to h^-\nu_\tau) = (12.18 \pm 0.33)\%$ [2, 4] after subtracting $B(\tau^- \to K^-\nu_\tau) = (0.65 \pm 0.06)\%$ [4, 6, 7]. The $\tau^- \to (5\pi)^-\nu_\tau$ contribution is the sum of $B(\tau^- \to 3h^-2h^+\nu_\tau) = (0.071 \pm 0.007)\%$ [4, 8], $B(\tau^- \to h^-h^+h^-2\pi^0\nu_\tau) = (0.52 \pm 0.05)\%$ [9] and $B(\tau^- \to h^-4\pi^0\nu_\tau) = (0.16 \pm 0.07)\%$ [10]. The $\tau^- \to e^-\bar{\nu}_e\nu_\tau$ branching ratio used for normalization is $(17.9 \pm 0.17)\%$ [4].

LEP between 1991 and 1994. These two semi-inclusive modes sum up to give all of the τ decays into 3-prongs and each is the main background in the determination of the other. Their branching ratios are extracted simultaneously from a sample of three charged track τ decays. The discrimination between decays with only charged hadrons and decays accompanied by one or more neutral pions is given by the ratio of the total energy deposited in the electromagnetic calorimeter to the sum of the track momenta. From the total three charged track sample, a measurement of the branching ratio of τ decays into 3-prongs is obtained. Using an event topology analysis, OPAL has previously measured the 3-prong branching ratio to be $(15.26 \pm 0.26 \pm 0.22)\%$ [16], which is significantly higher than the average branching ratio of other published results of $(13.98 \pm 0.24)\%$.[2] The result of this analysis is in agreement with and supersedes the previous OPAL measurement.

This paper is divided into the following parts: section 2 contains a brief description of the parts of the OPAL detector relevant to this analysis; section 3 describes the Monte Carlo used to simulate τ decays; section 4 outlines the selection of $e^+e^- \to \tau^+\tau^-$ and 3-prong τ decays and introduces the formalism used in calculating the $\tau^- \to h^-h^+h^-\nu_\tau$ and $\tau^- \to h^-h^+h^- \geq 1\pi^0\nu_\tau$ branching ratios; section 5 describes the corrections applied to the Monte Carlo predictions in order to obtain the final results; section 6 gives the details of the systematic error studies; and section 7 summarizes the results for the $\tau^- \to h^-h^+h^-\nu_\tau$, $\tau^- \to h^-h^+h^- \geq 1\pi^0\nu_\tau$ and $\tau^- \to$ 3-prong branching ratios and compares them to the present world averages.

2 The OPAL detector

A detailed description of the OPAL detector can be found elsewhere [17]. Only the characteristics of the subdetectors relevant to this analysis are given here. The OPAL coordinate system is defined with the origin at the nominal interaction point, the positive z axis along the e^- beam direction, the positive x axis in the beam plane pointing towards the center of the LEP ring and the positive y axis along the normal to the beam plane. The polar and azimuthal angles are called θ and ϕ, respectively.

The momentum and direction of charged particles are measured by a central tracking detector that contains three drift chambers: a vertex chamber, a large volume jet chamber with 159 layers of axial anode wires, and an outer chamber which provides a precise measurement of the z-coordinate. The three chambers are contained in a four bar pressure vessel and situated in a 0.435 T axial magnetic field. Combined, they provide a measurement of the particle momentum transverse to the beam direction, $\mathrm{p_t}$, with a resolution of $(\sigma_{\mathrm{p_t}}/\mathrm{p_t}) = \sqrt{(0.02)^2 + (0.0015\mathrm{p_t})^2}$ ($\mathrm{p_t}$ in GeV/c) for $|\cos\theta| < 0.73$. The jet chamber also provides a measurement of the energy loss of charged particles, dE/dx, with a resolution of approximately 3.5% for tracks in multihadronic events with the maximum number of hits used in the dE/dx calculation. Inside the vertex chamber is a small-radius silicon microvertex detector. Between 1992 and 1993, this detector was upgraded from one-coordinate to two-

[2] This value is obtained after subtracting the OPAL result from the world average branching ratio of reference [4] and includes a scale factor of S = 1.2. The averages of branching ratios used in this paper are calculated following the Particle Data Group unconstrained averaging procedure.

coordinate readout, thus allowing both $r\phi$ and z position measurements for charged tracks at radii of 61 and 75 mm [18].

Electromagnetic energy is measured by a lead glass electromagnetic calorimeter located outside the magnet coil, behind an average of two radiation lengths of material. Due to this upstream material, the intrinsic energy resolution of $\sigma_{\rm E}/{\rm E}$ = 5-6 $\%/\sqrt{\rm E}$ (E in GeV) is degraded by about a factor of two. In front of the lead glass calorimeter there is an array of 160 scintillators which acts as a time-of-flight counter, and a presampler detector which measures the position and multiplicity of particles entering the electromagnetic calorimeter. Further out in radius are a hadronic calorimeter of limited streamer tubes enclosed in the magnet return yoke, and a muon chamber system. The calorimetric detectors and muon chambers are divided into a cylindrical barrel region and two endcaps. A multi-element forward detector located in the small polar angle regions around the beam pipe measures the luminosity and completes the acceptance.

3 Monte Carlo simulation

A Monte Carlo simulation of the process $e^+e^- \to \tau^+\tau^-$ and of the subsequent τ decays is used to evaluate the efficiencies of the selection criteria described in sections 4 and 5. The $e^+e^- \to \tau^+\tau^-$ events were generated using the KORALZ 4.0 Monte Carlo [19]. The dynamics of the τ decays were simulated with the TAUOLA 2.4 decay library [20]. Bremsstrahlung photons from first order QED corrections to the τ decay modes are included when calculating the efficiencies of each channel. The Monte Carlo branching ratios for the channels not measured in this analysis were set equal to the values shown in Table 1.

A dedicated Monte Carlo sample was used to simulate the $\tau^- \to \pi^-\pi^+\pi^-\pi^0\nu_\tau$ final state. It implements a new parametrization of the hadronic matrix elements for the τ decay into four pseudoscalars [22]. Resonances with s-dependent coupling constants are added to the structure of the hadronic current. The coupling constants are tuned to obtain good agreement between the model and the experimental values of the $e^+e^- \to 4\pi$ cross-section in the center-of-mass energy range covered by the tau decay products ($\sqrt{s} = 1.0 - 2.0$ GeV). This parametrization was found to give a better description of the total track momentum and electromagnetic cluster energy distributions observed in the three charged track sample than the simpler model used in TAUOLA 2.4.

The Monte Carlo events were passed through the GEANT simulation [23] of the OPAL detector including a detailed simulation of the two-coordinate readout silicon microvertex detector [24]. The 1991-1992 data sample was collected with the one-coordinate readout silicon microvertex detector, which contains a different amount of material. Differences between the two versions of the silicon detector were checked with the data. We found that the fractions of conversion candidates in the silicon region in the 1991-1992 and the 1993-1994 data samples are consistent.

4 Event selection

The analysis is based on the data collected using the OPAL detector from 1991 through 1994 [3] for a total integrated luminosity of 128 pb^{-1}. About 80% of the integrated luminosity was recorded at the Z^0 peak, the remainder being taken at energy points within ± 3 GeV of the peak. Only data for which the tracking chambers and the electromagnetic calorimeter were fully operational are used.

4.1 Preselection of $e^+e^- \to \tau^+\tau^-$ events

The preselection of $e^+e^- \to \tau^+\tau^-$ candidate events [25, 26] is based on the very distinct signature of $\tau^+\tau^-$ pairs produced at the Z^0 energy: two nearly back-to-back jets with typically one to three charged particles and some missing energy due to the undetected neutrinos. Often in the event there are clusters in the electromagnetic calorimeter originating from neutral hadrons or photons which are not associated with any charged track. A jet is defined by assigning the charged tracks and the clusters in the electromagnetic calorimeter to cones of 35° half-angle [27]. A candidate tau pair event must have exactly two jets, each containing at least one charged track. The tracks and clusters considered in the jet definition must pass quality requirements. A track is accepted if it has a transverse momentum $p_t > 100$ MeV/c, an impact parameter in the plane perpendicular to the beam direction $d_0 < 2$ cm, a distance from the beam spot along the beam direction $z_0 < 75$ cm, and at least 20 measured points in the jet chamber with a maximum radius of 75 cm for the first wire hit. A cluster is accepted if it has an energy of at least 100 MeV in the barrel or 200 MeV in the endcap. Clusters in the endcap are also required to extend over a minimum of two lead glass blocks, each of them contributing less than 99% of the total cluster energy.

The multihadronic background is reduced by allowing a maximum of 6 charged tracks and 10 electromagnetic clusters in the event. The background from two-photon $e^+e^- \to (e^+e^-)X$ processes, where the final state e^+e^- escapes undetected at low angles and the system X is misidentified as a low visible energy τ pair event, is reduced by rejecting events with an acollinearity between the two charged jets greater than 15°. Further rejection is obtained by requiring that the total visible energy in the event, given by the sum over the two cones of the larger of either the scalar sum of track momenta or the summed cluster energy in each cone, exceeds 3% of the center-of-mass energy E_{cm}. Finally if the total visible energy is less than 20% of the center-of-mass energy, the event is rejected if the total transverse momentum of the charged tracks and transverse energy of the clusters in the event are both less than 2 GeV. Minor sources of backgrounds from cosmic rays and beam-gas interactions are suppressed with simple requirements on the location of the primary event vertex and on the time-of-flight signals associated with the tracks.

Decays of the Z^0 into charged leptons other than $\tau^+\tau^-$ can be identified by the presence of two very high momenta, back-to-back charged particles with the full beam energy deposited in

[3] About 6% of the 1994 data were collected after the silicon microvertex detector had been removed and are not considered in this analysis.

the electromagnetic calorimeter for $e^+e^- \to e^+e^-$ and with very little electromagnetic energy for $e^+e^- \to \mu^+\mu^-$. The $e^+e^- \to e^+e^-$ events are identified and rejected if either $E_{cls} > 0.7E_{cm}$ or $E_{cls} + 0.3p_{trk} > E_{cm}$, where E_{cls} is the total energy deposited in the lead glass calorimeter and p_{trk} is the total scalar momentum of the charged tracks. Muon pair events are identified by the combined use of the electromagnetic and hadronic calorimeters, and outer muon chambers [25, 26]. An event is classified and rejected as a muon pair if it contains at least two candidate muon tracks and if the scalar sum of the cluster energies plus the energy of the highest momentum track of both cones is greater than 60% of the center-of-mass energy.

After this preselection, a total of 87861 $\tau^+\tau^-$ candidate events are found in the barrel region of OPAL, defined by an average value of $|\cos\theta| < 0.68$ for the two jets. The residual non-τ contamination in the $\tau^+\tau^-$ sample, given by the sum of $e^+e^- \to e^+e^-$, $e^+e^- \to \mu^+\mu^-$, $e^+e^- \to q\bar{q}$ and two-photon $e^+e^- \to (e^+e^-)X$ events, was estimated from Monte Carlo studies and data control samples to be $f_{Bkgd}^{non-\tau} = (1.83 \pm 0.30)\%$ [26].

4.2 Selection of 3-prong τ decays

A significant component of background coming from 1-prong and 5-prong τ decays can be rejected simply by requiring that the preselected cones contain a number of charged tracks $N_{trk} = 3$. Poorly reconstructed cones can be further rejected, with minimal efficiency losses, by requiring that the sum of the charges of the three tracks is equal to ± 1. Monte Carlo studies indicate that the sample still has a considerable contamination from 1-prong τ decays containing an e^+e^- pair either from photon conversions ($20.07 \pm 0.17\%$) or from Dalitz decays of a π^0 ($2.61 \pm 0.07\%$), and from 1-prong $\tau^- \to h^- K_S^0 \geq 0\pi^0\nu_\tau$ decays with a $K_S^0 \to \pi^+\pi^-$ vertex close to the production point ($1.30 \pm 0.05\%$).[4] Minor sources of background come from 1-prong decays with two extra π/K tracks from nuclear interactions in the detector material and 5-prongs with two unreconstructed tracks.

Cones containing an e^+e^- pair from a photon converting in the detector material or from a Dalitz decay of a π^0 are identified and rejected on the basis of a topological conversion finder.[5] This finder looks for a conversion vertex defined as the point in the $r\phi$ plane where the tangents of two opposite sign tracks are parallel. The dE/dx of both tracks is required to be between 9.0 and 12 keV/cm, which is the typical energy loss of an electron. To reject accidental combinations of parallel tracks which do not come from a conversion vertex, the distance between the two tracks in the $r\phi$ plane at the conversion point is required to be less than 3 mm, the angular separation between the vector from the primary interaction point to the conversion point and the vector sum of the momenta of the candidate conversion tracks must be less than 5°, and the radius of the first hit in the jet chamber for both tracks must be no more than 20 cm before the conversion vertex.

To increase the selection efficiency for $\gamma \to e^+e^-$ conversions and for $\pi^0 \to e^+e^-\gamma$ decays, a conversion finder entirely based on dE/dx is also applied, thus exploiting the good particle

[4] Throughout the paper, the errors on Monte Carlo predictions are the Monte Carlo statistical errors, unless otherwise specified.

[5] In the following, e^+e^- pair production from a photon converting in the detector material or a Dalitz decay of a π^0 will be generically indicated as conversions, unless otherwise specified.

identification provided by the ionization energy loss for low momentum tracks. Two oppositely charged tracks in a cone are identified as an e^+e^- pair if both tracks have a momentum and an energy loss such that $(8.0 + 0.3\mathrm{p}) < \mathrm{dE/dx} < 12.0$, where p is measured in units of GeV/c and dE/dx is measured in units of keV/cm. The Monte Carlo predicts that the combination of the topological and dE/dx-based finders identifies $(94.33 \pm 0.23)\%$ of the $\mathrm{N_{trk}} = 3$ cones containing a $\gamma \to e^+e^-$ vertex and $(77.94 \pm 1.11)\%$ of the cones containing a $\pi^0 \to e^+e^-\gamma$ vertex. The larger inefficiency for the latter background arises from an inadequate modelling of the dynamics of Dalitz decays in the Monte Carlo, as discussed in section 5.2. Of the conversion candidates, $(84.82 \pm 0.33)\%$ come from $\gamma \to e^+e^-$ vertices, $(9.12 \pm 0.26)\%$ from $\pi^0 \to e^+e^-\gamma$ vertices and $(6.06 \pm 0.22)\%$ from fake conversions. The loss of efficiency of real 3-prong events is $(1.43 \pm 0.05)\%$.

The 1-prong $\tau^- \to h^- K^0_S \geq 0\pi^0\nu_\tau$ decays, in which $K^0_S \to \pi^+\pi^-$, are identified by the presence of a neutral secondary vertex in the cone. The neutral vertex is defined as the intersection of a pair of oppositely charged tracks in the plane perpendicular to the beam direction. To reduce the combinatorial background, quality cuts are imposed on the tracks and on the radius of the secondary vertex. In particular the requirement that the impact parameter of both tracks be further than 3 mm from the average beam spot eliminates most of the combinatorial background [28]. The invariant mass of the two tracks, assuming them both to be pions, is required to be between 400 and 600 MeV/c^2, consistent with the K^0_S mass. A sample containing $(41.3 \pm 1.9)\%$ of the cones with a $K^0_S \to \pi^+\pi^-$ vertex and having a purity of $(78.3 \pm 2.2)\%$, according to the Monte Carlo, is selected with these criteria, after the conversion rejection has been applied. In the data, 259 cones are identified as containing a $K^0_S \to \pi^+\pi^-$ vertex, compared with 193 ± 10 in the Monte Carlo. The disagreement is consistent with the large uncertainty in the $\tau^- \to h^- K^0_S \geq 0\pi^0\nu_\tau$ branching ratio and has been taken into account in the evaluation of the final systematic error.

After the 3-prong selection, the background from τ sources other than 3-prong decays has been reduced to $(3.72 \pm 0.09)\%$, according to the Monte Carlo. The different components of this residual contamination are summarized in table 2. The only expected non-τ background in the 3-prong sample comes from low multiplicity multihadronic jets. This contribution has been evaluated using a sample of 2.4 million $e^+e^- \to q\bar{q}$ events, generated with the JETSET 7.3 Monte Carlo [29] and passed through the OPAL full detector simulation [24]. The residual multihadronic contamination after the complete event selection is then estimated to be $(0.79 \pm 0.04)\%$. The contributions to the background from other non-τ sources such as two-photon events, $e^+e^- \to e^+e^-(\gamma)$ or $e^+e^- \to \mu^+\mu^-(\gamma)$ events with a converting photon, and $e^+e^- \to \ell^+\ell^- V$ events, with a pair of oppositely charged tracks that are not conversion electrons forming the V vertex, are found to be negligible.

4.3 Discrimination between $\tau^- \to h^-h^+h^-\nu_\tau$ and $\tau^- \to h^-h^+h^- \geq 1\pi^0\nu_\tau$ decays

Having selected a clean sample of 3-prong τ decays, we use the distribution of the total energy deposited in the electromagnetic calorimeter divided by the scalar sum of the momenta of the three tracks, E/p, to discriminate between the $\tau^- \to h^-h^+h^-\nu_\tau$ and $\tau^- \to h^-h^+h^- \geq 1\pi^0\nu_\tau$

modes. Figure 1a compares the E/p distribution of data to that of the Monte Carlo simulation for cones passing the 3-prong selection. There is good agreement for E/p > 0.1, the χ^2 probability for the Monte Carlo distribution being 32%. The discrepancy for values of E/p below 0.1 is due to the imperfect simulation of the interaction of minimum ionizing hadrons in the electromagnetic calorimeter, as discussed in section 6.

Using a cut on the E/p distribution, one can divide the 3-prong sample into $3h$-enhanced and $3h{\geq}1\pi^0$-enhanced samples. For each sample an equation can be written relating the efficiencies for selecting a particular channel, weighted by its branching ratio, and the number of candidates found in the data. The $\tau^- \to h^-h^+h^-\nu_\tau$ and $\tau^- \to h^-h^+h^- {\geq} 1\pi^0\nu_\tau$ branching ratios, for which the shorthand notation B_{3h} and $B_{3h\geq 1\pi^0}$ is used, can then be calculated by solving the system of equations:

$$\epsilon^{(1)}_{3h} B_{3h} + \epsilon^{(1)}_{3h\geq 1\pi^0} B_{3h\geq 1\pi^0} + \epsilon^{(1)}_{Bkgd} \cdot (1 - B_{3h} - B_{3h\geq 1\pi^0}) = \frac{N_1\,(1 - f_1^{non-\tau})}{N_\tau\,(1 - f_{Bkgd}^{non-\tau})} \qquad (1)$$

$$\epsilon^{(2)}_{3h} B_{3h} + \epsilon^{(2)}_{3h\geq 1\pi^0} B_{3h\geq 1\pi^0} + \epsilon^{(2)}_{Bkgd} \cdot (1 - B_{3h} - B_{3h\geq 1\pi^0}) = \frac{N_2\,(1 - f_2^{non-\tau})}{N_\tau\,(1 - f_{Bkgd}^{non-\tau})} \qquad (2)$$

where the index (1) indicates the $3h$-enhanced sample and the index (2) indicates the $3h{\geq}1\pi^0$-enhanced sample. The $\epsilon^{(i)}_{3h}$ and $\epsilon^{(i)}_{3h\geq 1\pi^0}$ terms are the Monte Carlo efficiencies for the $\tau^- \to h^-h^+h^-\nu_\tau$ and $\tau^- \to h^-h^+h^- {\geq} 1\pi^0\nu_\tau$ channels, calculated as explained in the following section. The $\epsilon^{(i)}_{Bkgd}$ are the Monte Carlo efficiencies of any residual non-3-prong τ decay, weighted by a term that constrains the sum of all τ branching ratios to be equal to 100%. The N_i are the number of 3-prong cones selected in the data and $f_i^{non-\tau}$ are the fractions of background events from sources other than τ decays in each E/p sample. Finally, N_τ is the total number of preselected cones in the data and $f_{Bkgd}^{non-\tau}$ is the non-τ background fraction in the preselected sample.

Solving the system of equations above for different values of the cut in the E/p distribution, we find that B_{3h} varies as shown in Figure 1b. The solution for $B_{3h\geq 1\pi^0}$ is constrained by the requirement that the two be equal to the measured $\tau^- \to$ 3-prong branching ratio. There is good stability for a large range of E/p. The high branching ratio for the first point reflects the discrepancy between Monte Carlo and data for low E/p values. The minimum statistical error is found for a cut on E/p at 0.6 which is chosen as the point of maximum discrimination between the two channels. The B_{3h} and $B_{3h\geq 1\pi^0}$ solutions found for this cut are in agreement with the values found from a χ^2-minimization of the E/p Monte Carlo distributions for the two decay modes with respect to the data distribution.

5 Efficiency calculation

The $\tau^- \to h^-h^+h^-\nu_\tau$ and $\tau^- \to h^-h^+h^- {\geq} 1\pi^0\nu_\tau$ decays, although dominated by the $\tau^- \to \pi^-\pi^+\pi^-\nu_\tau$ and $\tau^- \to \pi^-\pi^+\pi^-\pi^0\nu_\tau$ modes, have significant contributions from other 3-prong final states. Modes containing one or two kaons in the final state have been observed by the DELCO and TPC Collaborations [12, 13]. From the average of their results we expect a branching ratio of $(0.41 \pm 0.18)\%$ (S=1.8) for the $\tau^- \to K^-\pi^+\pi^-\nu_\tau$ channel

and $(0.17 \pm 0.07)\%$ (S=1.0) for the $\tau^- \to K^-K^+\pi^-\nu_\tau$ channel. The $\tau^- \to h^-h^+h^-2\pi^0\nu_\tau$ final state has been observed by CLEO [9]. Using their result for the ratio of $B(\tau^- \to h^-h^+h^-2\pi^0\nu_\tau)/B(\tau^- \to$ 3-prong) and the τ into 3-prongs branching fraction measured by OPAL [16], a branching ratio of $(0.52\pm0.05)\%$ is derived for the $\tau^- \to h^-h^+h^-2\pi^0\nu_\tau$ channel. A limit on potential contributions from $\tau^- \to h^-h^+h^-3\pi^0\nu_\tau$ decays of $(0.15\pm0.05)\%$ is obtained from the CVC predicted rate of τ into six pions [5], after subtracting the $\tau^- \to 3h^-2h^+\pi^0\nu_\tau$ contribution of Table 1.

In this analysis no attempt has been made to distinguish between pion and kaon tracks. Also the granularity of the OPAL electromagnetic calorimeter is not sufficient to distinguish in an unambiguous way decays with one or more π^0 on an event-by-event basis. Monte Carlo studies indicate that the efficiency of the 3-prong selection for $\tau^- \to K^-\pi^+\pi^-\nu_\tau$, $\tau^- \to K^-K^+\pi^-\nu_\tau$ and $\tau^- \to h^-h^+h^- \geq 2\pi^0\nu_\tau$ modes is significantly different from the efficiency of the dominant decays, as shown in Table 3. To account for this, assumptions have been made about the relative contribution of the non-dominant channels to the $\tau^- \to h^-h^+h^-\nu_\tau$ and $\tau^- \to h^-h^+h^- \geq 1\pi^0\nu_\tau$ final states based on the experimental measurements and phenomenological predictions above. Under the hypothesis that the $\tau^- \to h^-h^+h^-\nu_\tau$ and $\tau^- \to h^-h^+h^- \geq 1\pi^0\nu_\tau$ channels consist only of the $\tau^- \to \pi^-\pi^+\pi^-\nu_\tau$ and $\tau^- \to \pi^-\pi^+\pi^-\pi^0\nu_\tau$ decays, the solutions of the system of equations 1 and 2 are $B_{3h} = 9.65\%$ and $B_{3h\geq1\pi^0} = 5.26\%$. Based on these approximate branching ratios, a $\tau^- \to K^-\pi^+\pi^-\nu_\tau$ relative contribution of $(4\pm2)\%$ and a $\tau^- \to K^-K^+\pi^-\nu_\tau$ relative contribution of $(2\pm1)\%$ to the three charged final state are allowed. For the multiple π^0 final state, a $(10\pm1)\%$ relative contribution from $\tau^- \to h^-h^+h^-2\pi^0\nu_\tau$ decays is assumed. The final $\tau^- \to h^-h^+h^-\nu_\tau$ and $\tau^- \to h^-h^+h^- \geq 1\pi^0\nu_\tau$ efficiencies of Table 3 are then calculated as the weighted sums of the Monte Carlo efficiencies of all the above decays. The uncertainties on the different relative contributions are used in the evaluation of the systematic error. A separate systematic uncertainty is calculated by allowing a 3% relative contribution from the $\tau^- \to h^-h^+h^-3\pi^0\nu_\tau$ mode to the multiple π^0 final state. Since in this analysis no explicit π^0 reconstruction is attempted, the final results might be sensitive to the presence of other neutral mesons, like the η, whose decays include photons or π^0's. However, there is no experimental evidence for such final states in 3-prong τ decays and their branching ratios are expected to be small [30].

Also entering the system of equations in B_{3h} and $B_{3h\geq1\pi^0}$ are the background selection efficiencies, $\epsilon^{(i)}_{Bkgd}$. They are given by the sum of the Monte Carlo efficiencies of all τ channels that do not contribute to the 3-prong final state, weighted by the branching ratios of Table 1.

5.1 Signal efficiency correction

Of the 3-prong selection criteria, the requirement $N_{trk}=3$ causes the largest efficiency losses for signal channels, rejecting more than 13% of $\tau^- \to h^-h^+h^-\nu_\tau$ decays and more than 20% of $\tau^- \to h^-h^+h^- \geq 1\pi^0\nu_\tau$ decays. Decays with 3-prongs are lost to the $N_{trk}=2$ class because of track merging effects. Migration to topologies with $N_{trk}>3$ is due to track splitting effects or to the presence of a conversion. Table 4 gives the efficiencies of each category for $\tau^- \to h^-h^+h^-\nu_\tau$ and $\tau^- \to h^-h^+h^- \geq 1\pi^0\nu_\tau$ decays, as calculated from the Monte Carlo. These values were checked with control samples in the $N_{trk}=2$ and $N_{trk}>3$ topologies, as explained below.

Two problems are found to affect the number of reconstructed tracks in a cone: an unresolved left-right ambiguity in assigning hits to high momentum tracks which pass very close to the jet chamber anode plane, and an imperfect modelling in the Monte Carlo of the jet chamber double hit resolution. The left-right ambiguity causes spurious tracks with typically fewer than 60 wire hits to be reconstructed within 0.5° of the anode plane. This problem affects the relative number of 3-prong decays reconstructed in the $N_{trk} = 3$ and $N_{trk} = 4$ topologies and is considered in the calculation of the final systematic error of section 6. The double hit resolution is a measure of the probability with which the track reconstruction algorithm can resolve two nearby hits in the tracking chamber. In the data, this probability starts rising sharply at a hit separation of 1.5 mm and reaches 100% for distances around 4 mm. In the Monte Carlo, the same probability is reached only at 0.5-1.0 mm larger hit separations. This imperfect modelling of the double hit resolution affects the fraction of 3-prong events which are assigned to the $N_{trk} = 2$ class. Since one of the preselection cuts for good charged tracks requires that the innermost wire hit is within 75 cm of the beam axis, two close tracks in the $N_{trk} = 3$ sample which start having separate hits in the data at a radius around 75 cm have a lower probability to be resolved in the Monte Carlo and preferentially populate the $N_{trk} = 2$ class. In support of this interpretation we observe that the Monte Carlo minimum azimuthal separation between any two tracks in $N_{trk} = 3$ cones has a deficit with respect to the data in the low angle region.

To assign a correction to the $\tau^- \to h^-h^+h^-\nu_\tau$ and $\tau^- \to h^-h^+h^- \geq 1\pi^0\nu_\tau$ efficiencies due to this imperfect modelling of the double hit resolution, one has to identify cones in the $N_{trk} = 2$ class coming from 3-prong decays with two close unresolved tracks. Natural candidates are events for which one of the two tracks has an ionization energy loss of twice that of an isolated track. The energy loss of a charged particle of momentum $p > 100$ MeV/c is typically between 6 and 12 keV/cm. Therefore, we can select 2-prong cones with two close unresolved tracks by requiring that the dE/dx of either track is larger than 12 keV/cm. Monte Carlo studies indicate that the purity of real 3-prong τ decays in this sample can be increased to 95% by requiring that both tracks have an associated hit in the silicon microvertex detector, thus suppressing the background from 1-prong decays with a partially reconstructed conversion. There is a clear excess of events in the Monte Carlo sample relative to the data, indicating a larger loss of 3-prong decays to the $N_{trk} = 2$ class. The corresponding corrections to $\epsilon^{(i)}_{3h}$ and $\epsilon^{(i)}_{3h\geq 1\pi^0}$ are 1.017 ± 0.006 and 1.014 ± 0.006, respectively. The error on the correction takes into account the statistical precision of the $N_{trk} = 2$ sample and small discrepancies between data and Monte Carlo for the variables used in selecting this sample. The $\tau^- \to h^-h^+h^-\nu_\tau$ and $\tau^- \to h^-h^+h^- \geq 1\pi^0\nu_\tau$ efficiencies of Table 3 are corrected by these factors before being used in the calculation of the final branching ratios.

The fraction of 3-prong τ decays lost to the $N_{trk} > 3$ class due to γ conversions or Dalitz decays has been checked with a sample of $N_{trk} = 5$ cones with exactly two tracks identified as coming from a conversion. The conversion identification uses a combination of geometrical and energy loss requirements similar to the one used in selecting $\gamma \to e^+e^-$ and $\pi^0 \to e^+e^-\gamma$ decays in three charged-track cones. The $N_{trk} = 5$ sample is approximately 86% pure in $\tau^- \to h^-h^+h^- \geq 1\pi^0\nu_\tau$ decays, according to the Monte Carlo. The finder selects 544 cones in the data compared to 545 ± 29 in the Monte Carlo. The error is given by the combination of the Monte Carlo statistical error and the uncertainty in the final number of conversions discussed at the end of section 5.2. Given the good agreement, no corrections are applied to the $\tau^- \to h^-h^+h^-\nu_\tau$ and $\tau^- \to h^-h^+h^- \geq 1\pi^0\nu_\tau$ efficiencies for losses to topologies with $N_{trk} > 3$.

5.2 Background efficiency correction

The most effective cut against 1-prong decays in the $N_{trk} = 3$ sample is given by the combination of the topological and dE/dx-based conversion finders introduced in section 4.2. The number of cones containing an identified conversion, N_{conv}, can be written as:

$$N_{conv} = N_{e^+e^-}\epsilon_{conv} + N_{fake} \tag{3}$$

where $N_{e^+e^-}$ is the total number of cones with a conversion vertex, ϵ_{conv} is the conversion finder efficiency, and N_{fake} is the number of misidentified conversions. Even after the conversion rejection, 1-prong decays with an e^+e^- pair originating either from a γ conversion or from a π^0 Dalitz decay represent the main residual background to the 3-prong sample. This conversion background, which can be written as $N_{conv}^{Bkgd} = N_{e^+e^-} \cdot (1 - \epsilon_{conv})$, is affected by discrepancies in the Monte Carlo simulation either of the number of cones with a conversion vertex or the efficiency of detecting conversions. Detailed studies have been performed in order to check the final conversion contamination in the selected 3-prong decay sample.

The fraction of fake conversions, N_{fake}/N_{conv}, is predicted by the Monte Carlo to be around 6.1%, as seen in section 4.2. Most of the misidentified cones come from real 3-prong decays and their contribution has been checked by looking at the invariant mass distribution of the two tracks forming the conversion vertex, assuming that the particles are electrons. There is a $(21\pm9)\%$ excess relative to the data in the Monte Carlo invariant mass region above 0.4 GeV/c^2, where one expects to find most of the real 3-prong decays according to the Monte Carlo. Since the total fraction of 3-prongs misidentified as 1-prong decays with a conversion is predicted to be only 1.7% of the selected 3-prong decay candidates, the effect of this correction on $\epsilon_{3h}^{(i)}$ and $\epsilon_{3h\geq1\pi^0}^{(i)}$ is small and is included as a systematic uncertainty on the final $\tau^- \to h^-h^+h^-\nu_\tau$ and $\tau^- \to h^-h^+h^- \geq 1\pi^0\nu_\tau$ branching ratios.

The Monte Carlo efficiency of the $\gamma \to e^+e^-$ selection has been checked with the data using an enhanced sample of decays with a photon conversion. This sample was selected by requiring that only one of the three tracks have an associated hit in the silicon microvertex detector and that the remaining two tracks have an invariant mass, assuming the electron mass for both, less than 0.2 GeV/c^2. The purity of this sample is estimated from the Monte Carlo to be $(96.9 \pm 0.4)\%$, after correcting for inconsistencies between data and Monte Carlo in the association of silicon hits to the tracks and in the invariant mass distribution of 3-prong τ decays. Upon applying the normal conversion selection to this enhanced photon conversion sample, $(87.78 \pm 0.53)\%$ of the cones are identified in the data compared with $(91.69 \pm 0.64)\%$ in the Monte Carlo. A correction factor of 0.957 ± 0.009 is therefore applied to the Monte Carlo efficiency for selecting $\gamma \to e^+e^-$ vertices. Half of this correction is explained by an imperfect parametrization of the energy loss for electrons, as observed in an enhanced $\tau^- \to e^-\bar{\nu}_e\nu_\tau$ sample [26].

The Monte Carlo efficiency for $\pi^0 \to e^+e^-\gamma$ decays has been found to be affected by the inadequate modelling of the dynamics of π^0 Dalitz decays in GEANT 3.15 [23]. While the branching ratio is correctly set to 1.198% [4], the $\pi^0 \to e^+e^-\gamma$ decay is incorrectly treated as a three-body decay with sharing of momenta among the e^+, e^-, and the γ determined solely by phase space. The momentum spectrum of the electron and positron and their opening

angle, which are crucial quantities in the identification of e^+e^- pairs, are both affected by this approximate modelling, as confirmed by comparing the data and the Monte Carlo simulation for a sample enriched in $\pi^0 \to e^+e^-\gamma$ decays. The sample was selected by requiring that all three tracks in the cone have at least one associated silicon microvertex hit, that at least two of the tracks have a dE/dx value in the range from 9 to 12 keV/cm, and that the invariant mass of the e^+e^- pair is less than 0.15 GeV/c^2, consistent with the π^0 mass. After applying the conversion selection to this sample, a correction factor of 1.19 ± 0.08 is found for the Monte Carlo Dalitz conversion efficiency. The error on the correction comes from the sample statistics and from uncertainties in the amount of background from non-Dalitz decays.

Table 5 summarizes the corrections found for the $\gamma \to e^+e^-$ and $\pi^0 \to e^+e^-\gamma$ Monte Carlo efficiencies and their effects on the final conversion identification efficiency, $\epsilon_{\rm conv}$. The corresponding corrections to $\epsilon^{(1)}_{Bkgd}$ and $\epsilon^{(2)}_{Bkgd}$ are equal to 1.05 ± 0.03 and 1.18 ± 0.10, respectively. The difference reflects the different relative contributions of cones with a conversion vertex to the total number of background cones in the two E/p regions. The Monte Carlo efficiencies for the backgrounds in Table 3 have been corrected by these factors before being used in the calculation of the final branching ratios.

The number of cones with a conversion vertex, $N_{e^+e^-}$, is related both to the number of π^0 mesons produced in τ decays, since $\pi^0 \to \gamma\gamma$ and $\pi^0 \to e^+e^-\gamma$ decays represent the main source of photons in τ events, and to the amount of material that photons encounter in the tracking chambers. From the accuracy with which one knows the branching ratios of the 1-prong decay channels contributing most of the π^0 mesons, namely $\tau^- \to h^-\pi^0\nu_\tau$, $\tau^- \to h^-2\pi^0\nu_\tau$, and $\tau^- \to h^- \geq 3\pi^0\nu_\tau$, we derive a 3% uncertainty on $N_{e^+e^-}$. Uncertainties from 1-prong decays with an η meson in the final state, which are not modelled in the Monte Carlo, are expected to be small [30]. Possible effects from the modelling of bremsstrahlung photons from first order QED corrections to the τ decay modes have been checked by repeating the analysis ignoring any τ decay with such prompt photons. The final results do not show any significant changes.

The simulation of the material has been studied by looking at the distribution of the radial distance of conversion vertices from the beam spot in events identified by the combined topological and dE/dx finders. There is good qualitative agreement between the distribution of the conversion radii and the location of the material in front of the OPAL jet chamber. A correction to the Monte Carlo prediction for the total $N_{e^+e^-}$ using the data can be obtained from equation 3. For the term on the left-hand side, one compares the number of conversion candidates identified in data, $N^{\rm Data}_{\rm conv} = 6392$, with the number predicted by the Monte Carlo, $N^{\rm MC}_{\rm conv} = 6301 \pm 58$. For the terms on the right-hand side, differences between data and Monte Carlo for both $N_{\rm fake}$ and $\epsilon_{\rm conv}$ have been discussed previously. Therefore, the only unknown quantity in equation 3 is $N_{e^+e^-}$, for which one derives a correction factor of 1.05 ± 0.02. The changes induced on $\epsilon^{(1)}_{Bkgd}$ and $\epsilon^{(2)}_{Bkgd}$ by this correction are small and are included in the calculation of the systematic uncertainties affecting B_{3h} and $B_{3h\geq 1\pi^0}$.

5.3 Results

The values of all the parameters entering the equations 1 and 2 for a cut in E/p at 0.6 are shown in Table 6, where the corrections to the signal and background efficiencies discussed in the previous sections have been applied. The branching ratios derived from these parameters are $B_{3h} = 9.68\%$ and $B_{3h\geq 1\pi^0} = 4.93\%$. However, we must also correct for the preselection efficiencies, which are decay-mode dependent. The main reason for this dependence is due to the requirement of a maximum of 6 good charged tracks in the event, which rejects 3-prong τ decays where the opposite cone contains a 5-prong decay, a 3-prong τ decay with a conversion, or a τ decay with more than one conversion. Monte Carlo studies indicate that the bias induced by the preselection on the channels of interest in this analysis is $\mathrm{F}^{3h}_{\mathrm{Bias}} = 0.9805 \pm 0.0058$ and $\mathrm{F}^{3h\geq 1\pi^0}_{\mathrm{Bias}} = 0.9675 \pm 0.0075$, where the errors are the Monte Carlo statistical errors. Track reconstruction deficiencies not modelled in the Monte Carlo affect the preselection bias factors by much less than the uncertainties estimated above.

After dividing the $\tau^- \to h^-h^+h^-\nu_\tau$ and $\tau^- \to h^-h^+h^- \geq 1\pi^0\nu_\tau$ branching ratios calculated from the preselected sample by the bias factors above, we obtain:

$$\begin{aligned} B(\tau^- \to h^-h^+h^-\nu_\tau) &= (9.87 \pm 0.10)\% \\ B(\tau^- \to h^-h^+h^- \geq 1\pi^0\nu_\tau) &= (5.09 \pm 0.10)\% \end{aligned}$$

where the errors are statistical. The statistical correlation between the two measurements is -0.58. The branching ratio calculated from the total 3-prong selected sample is:

$$B(\tau^- \to \text{3-prong}) = (14.96 \pm 0.09)\%$$

where the error is statistical.

6 Systematic errors

The contributions to the systematic uncertainty in the determination of the $\tau^- \to h^-h^+h^-\nu_\tau$ and $\tau^- \to h^-h^+h^- \geq 1\pi^0\nu_\tau$ branching ratios are divided into three classes: contributions from the branching ratio extraction method, from the Monte Carlo simulation of the background, and from the calculation of the signal efficiencies. A summary is given in Table 7.

The efficiency terms in equations 1 and 2 have uncertainties due to the limited Monte Carlo statistics. One standard deviation statistical errors are propagated through the full matrix calculation. The uncertainties found for B_{3h} and $B_{3h\geq 1\pi^0}$ are both equal to $\pm 0.06\%$. The corrections to B_{3h} and $B_{3h\geq 1\pi^0}$ due to the decay-mode dependence of the τ preselection efficiency also give a systematic uncertainty on the final branching ratios. Changing the preselection bias factors by one standard deviation, we obtain variations in the $\tau^- \to h^-h^+h^-\nu_\tau$ and $\tau^- \to h^-h^+h^- \geq 1\pi^0\nu_\tau$ final branching ratios of $\pm 0.06\%$ and $\pm 0.04\%$, respectively.

Tests have been performed on the different sources of background surviving the 3-prong selection of table 2 in order to study possible systematic effects on the final branching ratios.

The background from 1-prong events with a $\gamma \to e^+e^-$ conversion or a $\pi^0 \to e^+e^-\gamma$ decay, which is the main contamination from τ sources, has been discussed in section 5.2. A discrepancy between data and Monte Carlo at the 5% level was found for the total number of cones with a conversion vertex, which corresponds to a change in the final B_{3h} and $B_{3h\geq 1\pi^0}$ of -0.01% and -0.02%, respectively. In addition, the systematic uncertainty on the conversion inefficiency correction induces a variation on the B_{3h} and $B_{3h\geq 1\pi^0}$ central values of $\pm 0.02\%$ and $\pm 0.07\%$, respectively. The sum in quadrature of these two variations is shown in Table 7 as the systematic error due to the conversion background.

The second main source of τ background in the final 3-prong sample is due to 1-prong $\tau^- \to h^- K^0_S \geq 0\pi^0\nu_\tau$ decays. After applying the $K^0_S \to \pi^+\pi^-$ selection, the numbers of events rejected in data and Monte Carlo were found to differ by $(34 \pm 11)\%$, where the error takes into account both the data and the Monte Carlo statistical errors. As a conservative estimate, the Monte Carlo prediction for the residual background from this source has been assigned a relative systematic error of $\pm 50\%$. This accounts also for potential contributions from the $\tau^- \to h^- K^0 \bar{K}^0 \nu_\tau$ channels which are not considered in this analysis. The changes to the final $\tau^- \to h^-h^+h^-\nu_\tau$ and $\tau^- \to h^-h^+h^- \geq 1\pi^0\nu_\tau$ branching ratios are equal to $\pm 0.05\%$ and $\pm 0.03\%$, respectively. A $\pm 50\%$ uncertainty has also been assigned to the background from 1-prong decays with a nuclear interaction, resulting in variations of $\pm 0.02\%$ and $\pm 0.07\%$ in the $\tau^- \to h^-h^+h^-\nu_\tau$ and $\tau^- \to h^-h^+h^- \geq 1\pi^0\nu_\tau$ branching ratios, respectively.

The residual multihadronic contamination after the complete event selection has been estimated by Monte Carlo studies to be $(0.79 \pm 0.04)\%$. It can be reduced by a factor of five simply by selecting events with only one track in the hemisphere opposite to a three-charged track decay. The $\tau^- \to h^-h^+h^-\nu_\tau$ and $\tau^- \to h^-h^+h^- \geq 1\pi^0\nu_\tau$ branching fractions calculated for this 3$-$1 topology are $(9.80 \pm 0.12)\%$ and $(5.12 \pm 0.12)\%$, respectively. The change to the B_{3h} and $B_{3h\geq 1\pi^0}$ central values is taken as an estimate of the systematic uncertainty due to the $e^+e^- \to q\bar{q}$ background. A minor source of systematic error is due to the uncertainty on the non-τ background fraction in the preselected $\tau^+\tau^-$ event sample. The change to the final $\tau^- \to h^-h^+h^-\nu_\tau$ and $\tau^- \to h^-h^+h^- \geq 1\pi^0\nu_\tau$ branching ratios induced by the one standard deviation variation of the $f^{non-\tau}_{Bkgd}$ fraction has been included in Table 7.

The Monte Carlo simulation of the distributions which affect the calculation of the $\tau^- \to h^-h^+h^-\nu_\tau$ and $\tau^- \to h^-h^+h^- \geq 1\pi^0\nu_\tau$ efficiencies has been checked in detail. Deficiencies in the Monte Carlo modelling of the track reconstruction algorithm have been discussed in section 5.1. Corrections of $(1.7 \pm 0.6)\%$ and $(1.4 \pm 0.6)\%$ were applied to the Monte Carlo predicted efficiencies of $\tau^- \to h^-h^+h^-\nu_\tau$ and $\tau^- \to h^-h^+h^- \geq 1\pi^0\nu_\tau$ decays to account for the imperfect modelling of the Monte Carlo double hit resolution. The systematic uncertainty on this correction results in an error of $\pm 0.06\%$ for B_{3h} and of $\pm 0.03\%$ for $B_{3h\geq 1\pi^0}$. A second effect on the determination of the $\tau^- \to h^-h^+h^-\nu_\tau$ and $\tau^- \to h^-h^+h^- \geq 1\pi^0\nu_\tau$ efficiencies is due to the presence in the data of a spurious fourth track close to the anode plane of the jet chamber. Selecting $N_{trk}=4$ cones which contain at least one track with fewer than 60 wire hits, we find 159 events in data compared with 59 ± 5 in the Monte Carlo. Adding these events to the final 3-prong sample, we observe a change of $+0.06\%$ in B_{3h} and $+0.01\%$ in $B_{3h\geq 1\pi^0}$. The final contribution to the systematic error from tracking modelling shown in Table 7 is the sum in quadrature of these two effects. The uncertainty of $\pm 0.11\%$ induced on the $\tau^- \to$ 3-prong branching ratio is the largest single systematic uncertainty on this quantity.

The quality of the Monte Carlo simulation of the energy deposited in the electromagnetic calorimeter by charged hadrons was investigated using a control sample of $\tau^- \to \pi^-\nu_\tau$ and $\tau^- \to K^-\nu_\tau$ decays [25]. A discrepancy is observed at very low energies $\mathrm{E/E_{beam}} < 0.02$ due to the imperfect modelling of the energy deposited by minimum ionizing particles. A discrepancy consistent with this observation can be seen in Figure 2, which shows the distribution of the total electromagnetic energy deposited by a $\tau^- \to h^-h^+h^-\nu_\tau$ enriched sample, selected by requiring that at least one $\pi^+\pi^-$ invariant mass combination is in the region of the $\rho(770)^0$ mass peak. To estimate the influence of this effect on the final branching ratios, a 15% gaussian smearing was applied to Monte Carlo hadronic energy in the region of $\mathrm{E/E_{beam}} < 0.16$ so as to obtain a good agreement with the data. The changes in the final B_{3h} and $B_{3h\geq 1\pi^0}$ branching ratios found after this smearing are equal to $+0.05\%$ and -0.05%, respectively, and are included in Table 7 as the low hadronic energy response contribution to the systematic uncertainty.

The final results are largely insensitive to the exact modelling of the energy resolution in the Monte Carlo but are affected by uncertainties in the calibration of the lead glass calorimeter, which can result in an overall energy scale discrepancy between data and Monte Carlo. The Monte Carlo energy scale uncertainty for the contribution to the total deposited energy from electromagnetic showers has been estimated to be $\pm 2\%$ at 1 GeV, decreasing to $\pm 0.5\%$ at 45 GeV. The Monte Carlo energy scale uncertainty for the contribution from hadronic showers has been evaluated using the difference between data and Monte Carlo in the average energy distribution of Figure 2. A 0.4% shift is observed for the region of $\mathrm{E/E_{beam}}$ between 0.1 and 0.4. Changing the Monte Carlo hadronic and electromagnetic energy scale by these factors, we find a maximum variation in the $\tau^- \to h^-h^+h^-\nu_\tau$ and $\tau^- \to h^-h^+h^- \geq 1\pi^0\nu_\tau$ branching ratios of $\pm 0.10\%$.

The final results depend critically on the simulation of the E/p distribution. The dependence of B_{3h} and $B_{3h\geq 1\pi^0}$ on the position of the E/p cut is taken as an estimate of the uncertainty in this simulation. Figure 1c shows the deviation of the $\tau^- \to h^-h^+h^-\nu_\tau$ branching ratio calculated at a given E/p cut, with respect to the value obtained for E/p at 0.6. Correlations between measurements are taken into account in calculating the error of each deviation. The r.m.s. of the deviations calculated for a set of cuts in the range 0.4–0.8 is found to be 0.12% for both decay modes. This range covers the region where the efficiencies of the $\tau^- \to h^-h^+h^-\nu_\tau$ and $\tau^- \to h^-h^+h^- \geq 1\pi^0\nu_\tau$ decay modes change the most rapidly and where a reduced sensitivity to the discrepancy between data and Monte Carlo in the low E/p region is expected. This discrepancy is already taken into account by the systematic error attributed to the low hadronic energy response. The r.m.s. deviation, whose stability has been checked for different sets of cuts in the 0.4–0.8 range, is assigned as a systematic error due to the E/p modelling. It is the largest single contribution to the systematic uncertainties of the $\tau^- \to h^-h^+h^-\nu_\tau$ and $\tau^- \to h^-h^+h^- \geq 1\pi^0\nu_\tau$ branching ratios and reflects the sensitivity of the measurement to the details of the modelling of the energy deposited by hadrons showering in the lead glass calorimeter.

In the calculation of $\epsilon_{3h}^{(i)}$ and $\epsilon_{3h\geq 1\pi^0}^{(i)}$, assumptions are made about the contribution of non-dominant modes to the $\tau^- \to h^-h^+h^-\nu_\tau$ and $\tau^- \to h^-h^+h^- \geq 1\pi^0\nu_\tau$ final states. The dependence of the final results on these assumptions has been evaluated by changing the contribution of each mode by twice the error given in section 5. In this way one accounts for inconsistencies between the different experimental results, especially in the $\tau^- \to K^-\pi^+\pi^-\nu_\tau$ channel [12, 13], and for possible biases in the determination of the $\tau^- \to h^-h^+h^-2\pi^0\nu_\tau$

branching ratio due to the assumed $B(\tau^- \to \text{3-prong})$. The resulting changes to B_{3h} and $B_{3h\geq 1\pi^0}$ are not very large, $\pm 0.04\%$ and $\pm 0.05\%$, respectively. A larger variation, equal to $+0.08\%$ for B_{3h} and -0.07% for $B_{3h\geq 1\pi^0}$, is found when the contribution from $\tau^- \to h^-h^+h^-3\pi^0\nu_\tau$ is included in the multi-π^0 final state. The discrepancy in the number of fake conversions found in section 5.2 slightly affects the $\tau^- \to h^-h^+h^-\nu_\tau$ and $\tau^- \to h^-h^+h^- \geq 1\pi^0\nu_\tau$ efficiencies and contributes systematic errors of 0.03% and 0.02% to the final B_{3h} and $B_{3h\geq 1\pi^0}$.

The sensitivity of the final results to the detailed Monte Carlo description of $\tau^- \to h^-h^+h^- \geq 1\pi^0\nu_\tau$ decays, in particular the $\tau^- \to \pi^-\pi^+\pi^-\pi^0\nu_\tau$ component, has been studied by comparing different Monte Carlo models. Using the simpler model implemented in the default version of the TAUOLA 2.4 decay library, which does not fit the observed total energy and momentum spectra as well as the model used in this analysis, we observe a change of only 0.01% to the final B_{3h} and $B_{3h\geq 1\pi^0}$. The Monte Carlo simulation of the E/p distribution has been tested directly against the data for an enhanced $\tau^- \to h^-h^+h^- \geq 1\pi^0\nu_\tau$ sample selected by requiring that two of the tracks in $\mathrm{N_{trk}}=5$ cones originate from an e^+e^- pair. There is good agreement in this distribution between data and Monte Carlo with 327 events found in the data with E/p > 0.6 compared to 303 ± 18 in the Monte Carlo, confirming that we do not expect a large dependence of the final results on the Monte Carlo modelling of $\tau^- \to h^-h^+h^- \geq 1\pi^0\nu_\tau$ decays.

7 Conclusions

A measurement of the branching ratios $\tau^- \to h^-h^+h^-\nu_\tau$ and $\tau^- \to h^-h^+h^- \geq 1\pi^0\nu_\tau$ has been performed using 87861 τ pair candidates collected with the OPAL detector near the $\mathrm{Z^0}$ peak. Using an analysis based on the ratio between the total energy and the scalar sum of the track momenta of τ decays with three charged tracks, the following results were obtained:

$$\begin{aligned} B(\tau^- \to h^-h^+h^-\nu_\tau) &= (9.87 \pm 0.10 \pm 0.24)\% \\ B(\tau^- \to h^-h^+h^- \geq 1\pi^0\nu_\tau) &= (5.09 \pm 0.10 \pm 0.23)\% \end{aligned}$$

where the first error is statistical and the second systematic. The statistical and systematic correlation between the two measurements are -0.58 and -0.56, respectively. In Figure 3 these results are compared with previously published measurements. The results of this analysis have a precision which is almost two times better than the precision of the current world averages.

The branching ratio calculated from the selected three charged track sample is:

$$B(\tau^- \to \text{3-prong}) = (14.96 \pm 0.09 \pm 0.22)\%$$

in agreement with, and superseding, the previous OPAL result of $(15.26 \pm 0.26 \pm 0.22)\%$ [16], with which only about 10% of the data are in common. This measurement is significantly higher than the average of the branching ratios measured by other experiments, $(13.98 \pm 0.24)\%$ [4].

In this analysis the results for $B(\tau^- \to h^-h^+h^-\nu_\tau)$, $B(\tau^- \to h^-h^+h^- \geq 1\pi^0\nu_\tau)$ and $B(\tau^- \to \text{3-prong})$ are all correlated. Measurements of the fraction of each semi-inclusive decay

mode in the total 3-prong sample have smaller systematic uncertainties. The results for the two fractions are:

$$\begin{aligned} B(\tau^- \to h^-h^+h^-\nu_\tau)/B(\tau^- \to \text{3-prong}) &= (0.660 \pm 0.004 \pm 0.014) \\ B(\tau^- \to h^-h^+h^- \geq 1\pi^0\nu_\tau)/B(\tau^- \to \text{3-prong}) &= (0.340 \pm 0.004 \pm 0.014) \end{aligned}$$

where the first error is statistical and the second systematic.

The $\tau^- \to h^-h^+h^-\nu_\tau$ branching ratio measured here is inconsistent with the present world average value of $(8.0 \pm 0.4)\%$ [4]. If contributions from final states with kaons [12, 13] are subtracted, we derive an exclusive $\tau^- \to \pi^-\pi^+\pi^-\nu_\tau$ branching ratio of $(9.29 \pm 0.26 \pm 0.19)\%$, where the first error is the experimental error of this measurement and the second is the uncertainty on the $\tau^- \to K^-\pi^+\pi^-\nu_\tau$ and $\tau^- \to K^-K^+\pi^-\nu_\tau$ branching ratios. This value is in agreement with the QCD prediction of $(9.0 \pm 0.5)\%$ obtained from calculations of the axial-vector component of the τ hadronic width [5]. It also agrees with the measured branching ratio of $(8.95 \pm 0.40)\%$ for $\tau^- \to \pi^-\pi^0\pi^0\nu_\tau$ [4, 6, 7], predicted to be the same as for $\tau^- \to \pi^-\pi^+\pi^-\nu_\tau$ decays, neglecting corrections of order m_π^2/m_τ^2 [11].

The result for the $\tau^- \to h^-h^+h^- \geq 1\pi^0\nu_\tau$ branching ratio is in good agreement with the world average of $(5.4 \pm 0.4)\%$ [4]. Upon subtraction of $B(\tau^- \to h^-h^+h^-2\pi^0\nu_\tau) = (0.52 \pm 0.05)\%$ [9] and ignoring potential $\tau^- \to h^-h^+h^-3\pi^0\nu_\tau$ contributions, we derive a $\tau^- \to h^-h^+h^-\pi^0\nu_\tau$ branching ratio of $(4.57 \pm 0.25 \pm 0.05)\%$, where the first error is the experimental error of this measurement and the second is the uncertainty on the $\tau^- \to h^-h^+h^-2\pi^0\nu_\tau$ measurement. This value is consistent with the CVC prediction for the three-charged pion plus one π^0 final state of $(4.8 \pm 0.7)\%$ [5].

Acknowledgements

We would like to thank M. Finkemeier for providing the Monte Carlo simulation code for the $\tau^- \to \pi^-\pi^+\pi^-\pi^0\nu_\tau$ decays used in this analysis.
It is a pleasure to thank the SL Division for the efficient operation of the LEP accelerator, the precise information on the absolute energy, and their continuing close cooperation with our experimental group. In addition to the support staff at our own institutions we are pleased to acknowledge the
Department of Energy, USA,
National Science Foundation, USA,
Particle Physics and Astronomy Research Council, UK,
Natural Sciences and Engineering Research Council, Canada,
Fussefeld Foundation,
Israel Ministry of Science,
Israel Science Foundation, administered by the Israel Academy of Science and Humanities,
Minerva Gesellschaft,
Japanese Ministry of Education, Science and Culture (the Monbusho) and a grant under the Monbusho International Science Research Program,
German Israeli Bi-national Science Foundation (GIF),

Direction des Sciences de la Matière du Commissariat à l'Energie Atomique, France,
Bundesministerium für Forschung und Technologie, Germany,
National Research Council of Canada,
A.P. Sloan Foundation and Junta Nacional de Investigação Científica e Tecnológica, Portugal.

References

[1] K. Hayes in Particle Data Group, L. Montanet et al.: Phys. Rev. D50 (1994) 1403, and references therein

[2] ALEPH Coll., D. Decamp et al.: Z. Phys. C54 (1992) 211

[3] ARGUS Coll., H. Albrecht et al.: Z. Phys. C58 (1993) 61

[4] Particle Data Group, L. Montanet et al.: Phys. Rev. D50 (1994) 1173

[5] S. Narison and A. Pich, Phys. Lett. B304 (1993) 359

[6] ALEPH Coll., D. Buskulic et al.: Phys. Lett. B332 (1994) 209

[7] CLEO Coll., M. Battle et al.: Phys. Rev. Lett. 73 (1994) 1079

[8] CLEO Coll., D. Gibaut et al.: Phys. Rev. Lett. 73 (1994) 934

[9] CLEO Coll., D. Bortoletto et al.: Phys. Rev. Lett. 71 (1993) 1791

[10] CLEO Coll., M. Procario et al.: Phys. Rev. Lett. 70 (1993) 1207

[11] J. J. Gomez-Cadenas, M. C. Gonzales-Garcia and A. Pich, Phys. Rev. D42 (1990) 3093

[12] DELCO Coll., G. B. Mills et al.: Phys. Rev. Lett. 54 (1985) 624

[13] TPC Coll., D. A. Bauer et al.: Phys. Rev. D50 (1994) 13

[14] S. I. Dolinsky et al.: Phys. Rep. 202 (1991) 99;
A. Antonelli et al.: Nucl. Phys. B212 (1988) 133;
G. Cosme et al.: Nucl. Phys. B152 (1979) 215;
G. Bacci et al.: Nucl. Phys. B184 (1981) 31

[15] S. I. Eidelman and V. N. Ivanchenko, Phys. Lett. B257 (1991) 437;
F. J. Gilman and S. H. Rhie, Phys. Rev. D31 (1985) 1066

[16] OPAL Coll., P. Acton et al.: Phys. Lett. B288 (1992) 373

[17] OPAL Coll., K. Ahmet et al.: Nucl. Instrum. Methods, A313 (1992) 103

[18] P. P. Allport et al.: Nucl. Instrum. Methods A324 (1993) 34;
P. P. Allport et al.: Nucl. Instrum. Methods A346 (1994) 476

[19] S. Jadach, B. F. L. Ward and Z. Was, Comput. Phys. Commun. 79 (1994) 503

[20] S. Jadach and Z. Was, Comput. Phys. Commun. 76 (1993) 361

[21] ALEPH Coll., D. Buskulic et al.: Phys. Lett. B332 (1994) 219

[22] R. Decker, M. Finkemeier, P. Heiliger, H. H. Jonsson: TTP94-13, (1994)

[23] R. Brun et al.: GEANT3 User's Guide, CERN DD/EE/84-1 (1989)

[24] J. Allison et al.: Nucl. Instrum. Methods A317 (1992) 47

[25] OPAL Coll., G. Alexander et al.: Phys. Lett. B266 (1991) 201

[26] OPAL Coll., R. Akers et al.: Z. Phys. C66 (1995) 543

[27] OPAL Coll., G. Alexander et al.: Z. Phys. C52 (1991) 175

[28] OPAL Coll., G. Alexander et al.: Phys. Lett. B264 (1991) 467

[29] T. Sjöstrand, Comput. Phys. Commun. 39 (1986) 347:
T. Sjöstrand and M. Bengtsson, Comput. Phys. Commun. 43 (1987) 367

[30] CLEO Coll., M. Artuso et al.: Phys. Rev. Lett. 69 (1992) 3278

[31] CELLO Coll., H. J. Behrend et al.: Z. Phys. C46 (1990) 537

[32] ARGUS Coll., H. Albrecht et al.: Phys. Lett. B185 (1987) 222

[33] DELCO Coll., W. Ruckstuhl et al.: Phys. Rev. Lett. 56 (1986) 2132

[34] MARK2 Coll., W. B. Schmidke et al.: Phys. Rev. Lett. 57 (1986) 527

[35] MAC Coll., E. Fernandez et al.: Phys. Rev. Lett. 54 (1985) 1624

[36] CELLO Coll., H. J. Behrend et al.: Phys. Lett. B127 (1984) 1944

Decay mode		Branching ratio (%)	Input Monte Carlo channels
$\tau^- \to e^-\bar{\nu}_e\nu_\tau$		17.90 $\pm$ 0.17	$\tau^- \to e^-\bar{\nu}_e\nu_\tau$
$\tau^- \to \mu^-\bar{\nu}_\mu\nu_\tau$		17.44 $\pm$ 0.23	$\tau^- \to \mu^-\bar{\nu}_\mu\nu_\tau$
$\tau^- \to h^-\nu_\tau$		12.18 $\pm$ 0.33	$\tau^- \to \pi^-\nu_\tau$, $\tau^- \to K^-\nu_\tau$
$\tau^- \to h^-\pi^0\nu_\tau$		25.4 $\pm$ 0.5	$\tau^- \to \rho^-(\pi^-\pi^0)\nu_\tau$, $\tau^- \to K^{*-}(K^-\pi^0)\nu_\tau$
$\tau^- \to h^-2\pi^0\nu_\tau$		9.0 $\pm$ 0.4	$\tau^- \to a_1^-(\pi^-2\pi^0)\nu_\tau$, $\tau^- \to K^-2\pi^0\nu_\tau$
$\tau^- \to h^- \geq 3\pi^0\nu_\tau$		1.31 $\pm$ 0.17	$\tau^- \to \pi^-3\pi^0\nu_\tau$
$\tau^- \to h^-K^0\nu_\tau$	(†)	1.22 $\pm$ 0.20	$\tau^- \to K^{*-}(\pi^-K^0)\nu_\tau$, $\tau^- \to K^-K^0\nu_\tau$
$\tau^- \to h^-K^0 \geq 1\pi^0\nu_\tau$	(†)	0.38 $\pm$ 0.17	$\tau^- \to \pi^-K^0\pi^0\nu_\tau$, $\tau^- \to K^-K^0\pi^0\nu_\tau$
$\tau^- \to 3h^-2h^+\nu_\tau$	(†)	0.071 $\pm$ 0.007	$\tau^- \to 3\pi^-2\pi^+\nu_\tau$
$\tau^- \to 3h^-2h^+\pi^0\nu_\tau$	(†)	0.022 $\pm$ 0.010	$\tau^- \to 3\pi^-2\pi^+\pi^0\nu_\tau$

Table 1: Branching ratios and input Monte Carlo modes for the τ decays not directly measured in this analysis. For the modes marked with a †, the branching ratios of reference [4] are averaged with recently published results. The $B(\tau^- \to h^-\nu_\tau)$ result from ALEPH is included in the average after subtracting the $\tau^- \to K^*(892)^-\nu_\tau, K^*(892)^- \to K^0_S\pi^-$ contribution [2]. The $\tau^- \to h^- \geq 3\pi^0\nu_\tau$ branching ratio is the sum of the $\tau^- \to h^-3\pi^0\nu_\tau$ and $\tau^- \to h^-4\pi^0\nu_\tau$ branching ratios [4,10]. The $\tau^- \to h^-K^0\nu_\tau$ branching ratio is the sum of $B(\tau^- \to \pi^-K^0\nu_\tau)$ (estimated as 2/3 of the $\tau^- \to K^*(892)^-\nu_\tau$ branching ratio [4]), and $B(\tau^- \to K^-K^0\nu_\tau)$ as measured by ALEPH [21]. The $\tau^- \to h^-K^0 \geq 1\pi^0\nu_\tau$ branching ratio is the sum of $B(\tau^- \to \pi^-K^0\pi^0\nu_\tau)$ and $B(\tau^- \to K^-K^0\pi^0\nu_\tau)$, both measured by ALEPH [21]. The $\tau^- \to h^-K^0\bar{K}^0\nu_\tau$ decay mode is not considered. The $\tau^- \to 3h^-2h^+\nu_\tau$ and $\tau^- \to 3h^-2h^+\pi^0\nu_\tau$ branching ratios include recent CLEO 5-prong measurements [8]

Source	Contamination (%)
τ decays:	
1-prong with $\gamma \to e^+e^-$ conversion	1.43 $\pm$ 0.06
1-prong with $\pi^0 \to e^+e^-\gamma$ decay	0.66 $\pm$ 0.04
1-prong with $K^0_S \to \pi^+\pi^-$ vertex	0.97 $\pm$ 0.05
1-prong with nuclear interaction	0.61 $\pm$ 0.04
5-prong	0.05 $\pm$ 0.01
Total τ decays	3.72 $\pm$ 0.09
Multihadronic decays	0.79 $\pm$ 0.04
Total	4.51 $\pm$ 0.10

Table 2: Background fractions from τ decays and from multihadronic events after the 3-prong selection. The errors are the Monte Carlo statistical errors

Decay mode	Monte Carlo efficiency (%)		
	3-prong selection	E/p < 0.6	E/p > 0.6
$\tau^- \to \pi^-\pi^+\pi^-\nu_\tau$	84.92 $\pm$ 0.21	77.75 $\pm$ 0.25	7.17 $\pm$ 0.15
$\tau^- \to K^-\pi^+\pi^-\nu_\tau$	85.13 $\pm$ 0.81	80.21 $\pm$ 0.91	4.92 $\pm$ 0.49
$\tau^- \to K^-K^+\pi^-\nu_\tau$	75.62 $\pm$ 2.40	72.81 $\pm$ 2.49	2.81 $\pm$ 0.92
$\tau^- \to h^-h^+h^-\nu_\tau$	84.75 $\pm$ 0.21	77.75 $\pm$ 0.24	7.00 $\pm$ 0.15
$\tau^- \to \pi^-\pi^+\pi^-\pi^0\nu_\tau$	77.58 $\pm$ 0.34	32.16 $\pm$ 0.38	45.42 $\pm$ 0.41
$\tau^- \to \pi^-\pi^+\pi^-2\pi^0\nu_\tau$	72.71 $\pm$ 1.20	10.77 $\pm$ 0.84	61.94 $\pm$ 1.31
$\tau^- \to \pi^-\pi^+\pi^-3\pi^0\nu_\tau$	69.86 $\pm$ 5.37	4.11 $\pm$ 2.32	65.75 $\pm$ 5.55
$\tau^- \to h^-h^+h^- \geq 1\pi^0\nu_\tau$	77.08 $\pm$ 0.33	30.02 $\pm$ 0.35	47.06 $\pm$ 0.39
$\tau^- \to$ non-3-prong	0.54 $\pm$ 0.01	0.17 $\pm$ 0.01	0.37 $\pm$ 0.02

Table 3: Uncorrected Monte Carlo efficiencies, relative to the number of preselected τ cones, for the 3-prong selection of exclusive channels contributing to the $\tau^- \to h^-h^+h^-\nu_\tau$ and $\tau^- \to h^-h^+h^- \geq 1\pi^0\nu_\tau$ final states. The $\tau^- \to h^-h^+h^-\nu_\tau$, $\tau^- \to h^-h^+h^- \geq 1\pi^0\nu_\tau$ and $\tau^- \to$ non-3-prong efficiencies are the weighted sums of different final states according to the assumptions of section 5. The errors shown are the Monte Carlo statistical errors

N_{trk}	$\epsilon_{3h}(\%)$	$\epsilon_{3h\geq 1\pi^0}(\%)$
1	0.48 $\pm$ 0.04	0.65 $\pm$ 0.08
2	11.30 $\pm$ 0.18	9.95 $\pm$ 0.23
3	86.68 $\pm$ 0.20	79.52 $\pm$ 0.32
4	1.13 $\pm$ 0.06	4.33 $\pm$ 0.16
5	0.41 $\pm$ 0.04	5.55 $\pm$ 0.18

Table 4: Efficiency for selecting $\tau^- \to h^-h^+h^-\nu_\tau$ and $\tau^- \to h^-h^+h^- \geq 1\pi^0\nu_\tau$ decays in final states of different charged multiplicities

Source	Uncorrected Monte Carlo efficiency (%)	Correction factor	Corrected Monte efficiency (%)
$\gamma \to e^+e^-$	94.33 $\pm$ 0.23	0.957 $\pm$ 0.009	90.27 $\pm$ 0.87
$\pi^0 \to e^+e^-\gamma$	77.94 $\pm$ 1.11	1.19 $\pm$ 0.08	92.75 $\pm$ 6.37
conversion	92.44 $\pm$ 0.24	0.980 $\pm$ 0.011	90.56 $\pm$ 1.04

Table 5: Summary of the corrections applied to the photon conversion and Dalitz decay identification efficiencies. The last line shows the correction for the overall conversion selection efficiency, that is for 3-prong decays containing either $\pi^0 \to e^+e^-\gamma$ or $\gamma \to e^+e^-$ vertices. The errors on the uncorrected Monte Carlo efficiencies are the Monte Carlo statistical error only. The errors on the corrected Monte Carlo predictions also include the systematic uncertainties on the correction factors

	E/p < 0.6	E/p > 0.6
$\epsilon_{3h}^{(i)}$ (%)	79.07 $\pm$ 0.47	7.12 $\pm$ 0.04
$\epsilon_{3h\geq 1\pi^0}^{(i)}$ (%)	30.44 $\pm$ 0.18	47.72 $\pm$ 0.28
$\epsilon_{Bkgd}^{(i)}$ (%)	0.18 $\pm$ 0.05	0.44 $\pm$ 0.04
N_i	16110	6018
$f_i^{non-\tau}$(%)	0.32 $\pm$ 0.03	2.04 $\pm$ 0.13

N_τ	175722
$f_{Bkgd}^{non-\tau}$ (%)	1.83 $\pm$ 0.30
$\mathrm{F}_{\mathrm{Bias}}^{3h}$	0.9805 $\pm$ 0.0058
$\mathrm{F}_{\mathrm{Bias}}^{3h\geq 1\pi^0}$	0.9675 $\pm$ 0.0075

Table 6: Parameters used in the calculation of the final $\tau^- \to h^-h^+h^-\nu_\tau$ and $\tau^- \to h^-h^+h^- \geq 1\pi^0\nu_\tau$ branching ratios. The $\epsilon_{3h}^{(i)}$, $\epsilon_{3h\geq 1\pi^0}^{(i)}$, and $\epsilon_{Bkgd}^{(i)}$ for the two E/p regions are corrected for the discrepancies discussed in sections 5.1 and 5.2. The errors are the combination of the Monte Carlo statistical errors and the systematic uncertainties on the correction factors. The $f_{Bkgd}^{non-\tau}$ is estimated from Monte Carlo studies and corrected using background-enhanced samples from the data. Its error is a combination of the statistical error of the control samples and the systematic uncertainties on the corrections derived from these samples. The errors on $f_i^{non-\tau}$, $\mathrm{F}_{\mathrm{Bias}}^{3h}$ and $\mathrm{F}_{\mathrm{Bias}}^{3h\geq 1\pi^0}$ are statistical only

Source	ΔB_{3h} (%)	$\Delta B_{3h\geq 1\pi^0}$ (%)	ΔB_3 (%)
Monte Carlo statistics	0.06	0.06	0.03
Preselection bias factor	0.06	0.04	0.10
Conversion background	0.02	0.07	0.05
$\tau^- \to h^-K_S^0 \geq 0\pi^0\nu_\tau$ background	0.05	0.03	0.08
1-prong with nuclear interaction background	0.02	0.07	0.05
3-prong non-τ background	0.07	0.03	0.04
$f_{Bkgd}^{non-\tau}$ background	0.03	0.02	0.05
Tracking modelling	0.08	0.03	0.11
Low hadronic energy response	0.05	0.05	-
Energy scale	0.10	0.10	-
E/p modelling	0.12	0.12	-
ϵ_{3h} and $\epsilon_{3h\geq 1\pi^0}$ determination	0.04	0.05	0.09
$\tau^- \to h^-h^+h^-3\pi^0\nu_\tau$ contribution	0.08	0.07	0.01
Fake conversion rejection	0.03	0.02	0.05
$\tau^- \to h^-h^+h^- \geq 1\pi^0\nu_\tau$ spectrum modelling	0.01	0.01	0.02
Total	0.24	0.23	0.22

Table 7: Summary of the systematic uncertainties for the B_{3h}, the $B_{3h\geq 1\pi^0}$, and the $\tau^- \to$ 3-prong branching ratio, B_3. The total systematic error is the sum in quadrature of the different contributions

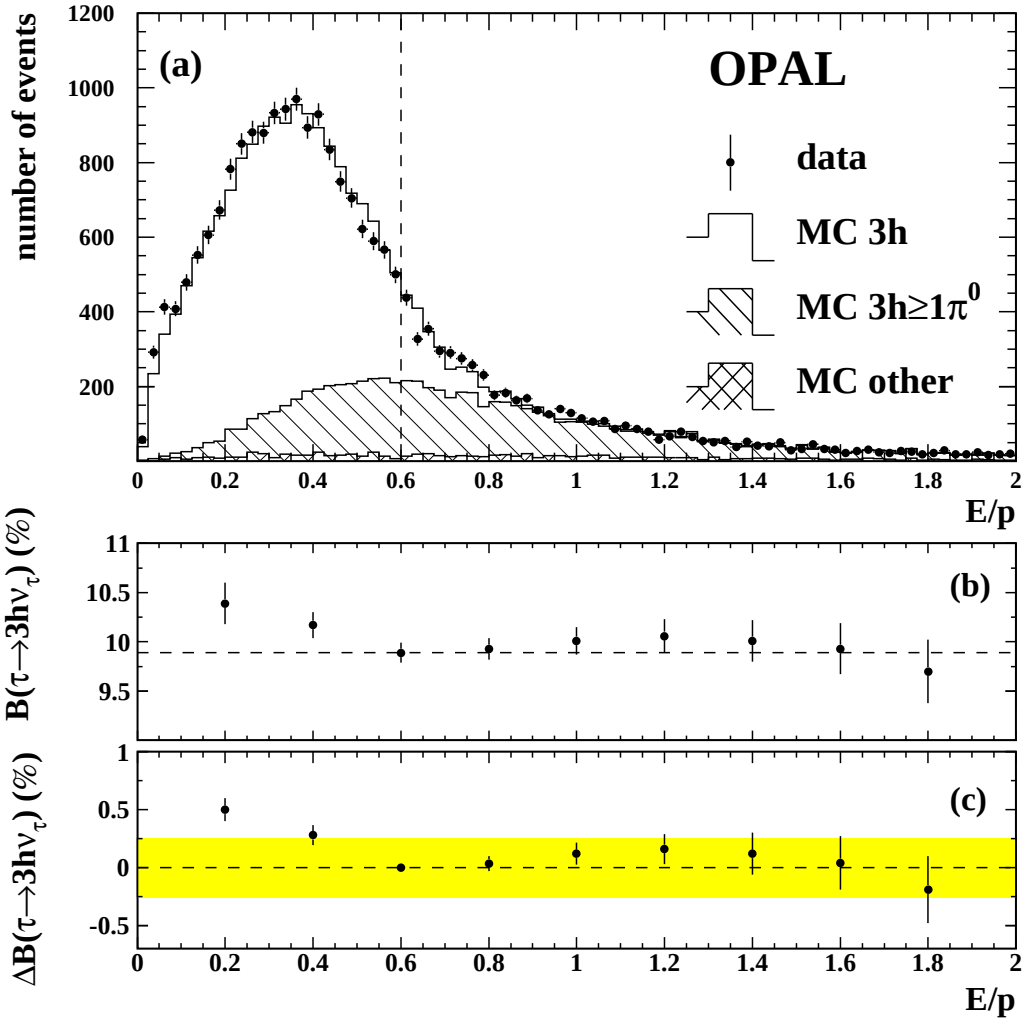

Figure 1: Plot (a) shows the E/p distribution for the selected 3-prong sample. The Monte Carlo (histogram) is normalized to the number of preselected τ cones observed in the data (points with error bars). The open area represents $\tau^- \to h^-h^+h^-\nu_\tau$ decays. The single hatched area shows the distribution for $\tau^- \to h^-h^+h^- \geq 1\pi^0\nu_\tau$ decays. The double hatched area shows the background from sources other than $\tau^- \to h^-h^+h^-\nu_\tau$ and $\tau^- \to h^-h^+h^- \geq 1\pi^0\nu_\tau$. The 3-prong Monte Carlo branching ratios have been reweighted to agree with the ones calculated in this analysis. The vertical dashed line indicates the location of the cut used to discriminate between $\tau^- \to h^-h^+h^-\nu_\tau$ and $\tau^- \to h^-h^+h^- \geq 1\pi^0\nu_\tau$ decays. Plot (b) shows the $\tau^- \to h^-h^+h^-\nu_\tau$ branching ratio for different values of the E/p cut. The errors are statistical. The horizontal dashed line shows the value of the branching ratio for a cut in E/p at 0.6. The high branching ratio for the first point reflects the discrepancy between Monte Carlo and data for low E/p values due to the imperfect simulation of the interaction of minimum ionizing hadrons in the electromagnetic calorimeter. Plot (c) shows the deviations between the $\tau^- \to h^-h^+h^-\nu_\tau$ branching ratio calculated at a given point and the one calculated for a cut in E/p at 0.6. The errors take into account the statistical correlations between the measurements. The shaded band shows the final value of the total error of the $B(\tau^- \to h^-h^+h^-\nu_\tau)$ measurement presented here

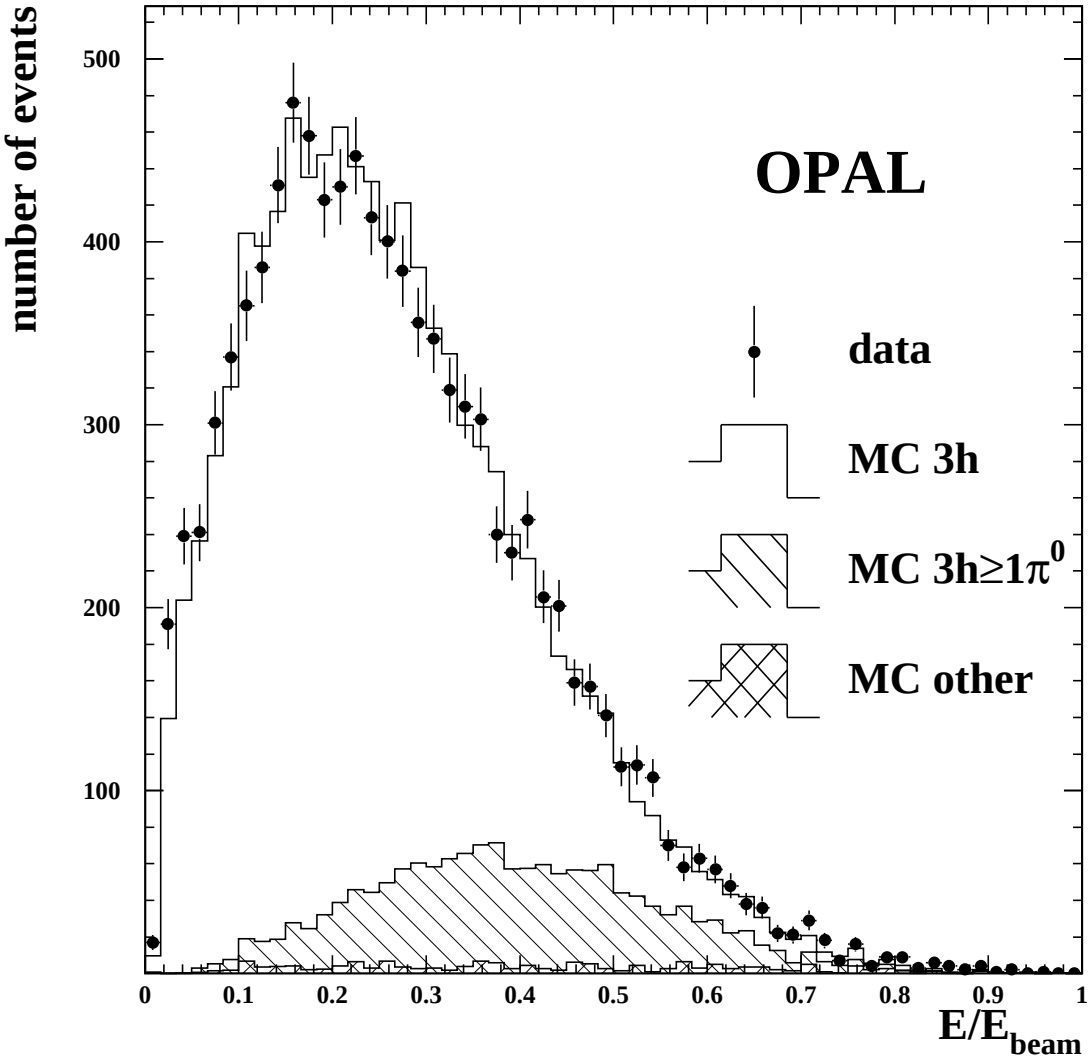

Figure 2: Total electromagnetic energy, normalized to the beam energy, for all 3-prong selected candidates in which at least one of the $\pi^+\pi^-$ invariant mass combinations is in the region of the $\rho(770)^0$ mass peak. The Monte Carlo (histogram) is normalized to the number of cones observed in the data (points with error bars). The open area is due to $\tau^- \to h^-h^+h^-\nu_\tau$ decays. The single hatched area shows events coming from $\tau^- \to h^-h^+h^- \geq 1\pi^0\nu_\tau$ decays. The double hatched area shows the background from sources other than $\tau^- \to h^-h^+h^-\nu_\tau$ and $\tau^- \to h^-h^+h^- \geq 1\pi^0\nu_\tau$. The 3-prong Monte Carlo branching ratios have been reweighted to agree with the ones calculated in this analysis

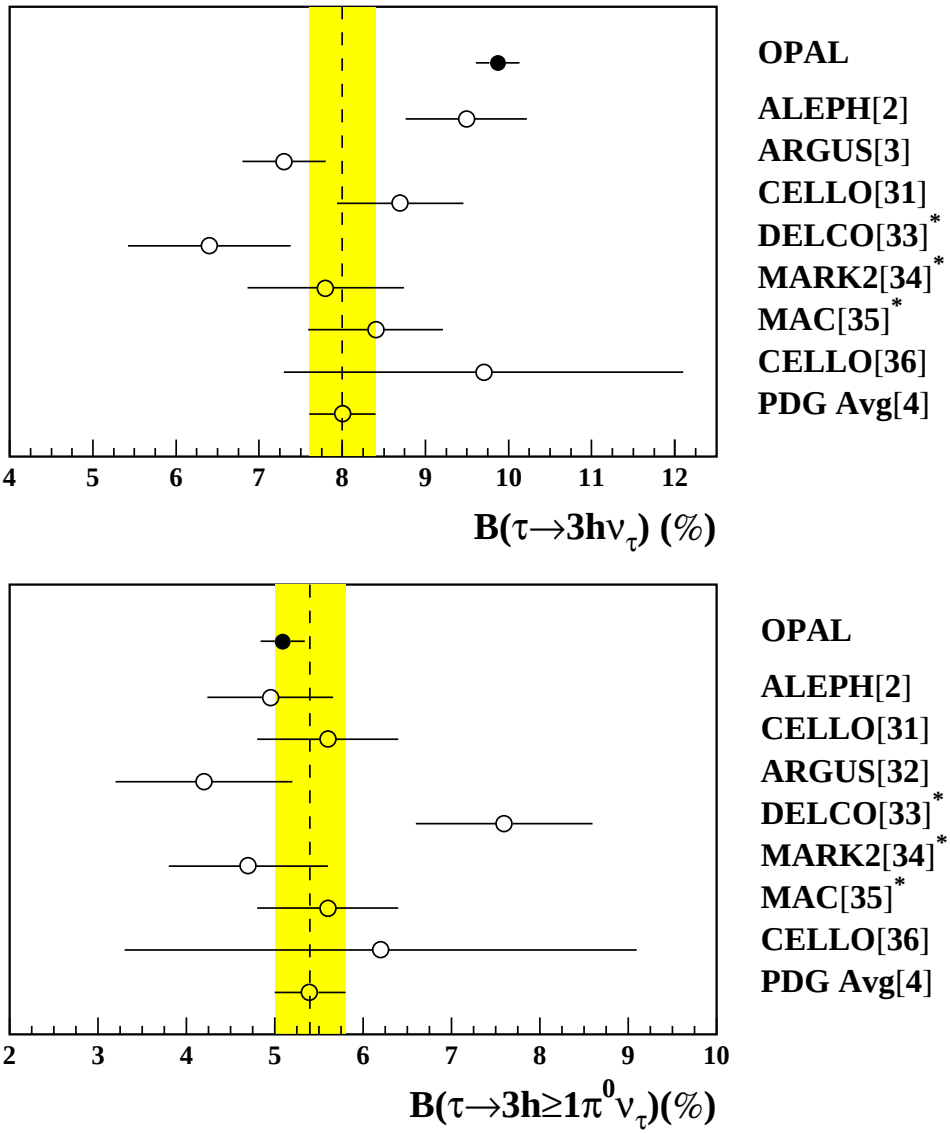

Figure 3: The branching ratios for $\tau^- \to h^-h^+h^-\nu_\tau$ and $\tau^- \to h^-h^+h^- \geq 1\pi^0\nu_\tau$ decays as measured by other experiments (open circles) compared with the results of this analysis (filled circles). The error bars give the sum of the statistical and systematic errors, when both are available. The dashed vertical lines are the world average values before this analysis [4]. The shaded areas show the error of the world averages. The measurements marked with an asterisk are calculated using the current Particle Data Group fit value of $B(\tau \to \text{3-prong}) = 0.1438$ [4]